THESIS FOR THE DEGREE OF LICENTIATE OF PHILOSOPHY

Dark matter electron interactions in detector materials

Einar Urdshals

CHALMERS
UNIVERSITY OF TECHNOLOGY

Department of Physics
Chalmers University of Technology
Gothenburg, Sweden, 2023

Dark matter electron interactions in detector materials

Einar Urdshals

Technical Report No. 1111-111X
ISSN 3.1415-9265
This thesis has been prepared using LaTeX.

Department of Physics
Chalmers University of Technology
SE-412 96 Gothenburg, Sweden
Phone: +46 (0)702365597
www.chalmers.se

Printed by Chalmers Reproservice
Gothenburg, Sweden, January 2023

Dark matter electron interactions in detector materials
Einar Urdshals, Department of Physics
Chalmers University of Technology

Abstract

Dark Matter (DM) makes up 85% of the matter content of the universe, and its gravitational effects are seen on scales ranging from that of cosmology to that of galactic astrophysics. The nature of DM is, however, unknown. Studying DM in the lab is key to understanding its nature. For decades, experiments have been attempting to do this through searches for DM induced nuclear recoils. These have not been found, and a possible reason for this is that the hypothetical DM particle is too light to induce nuclear recoils. Therefore, in the last decade experiments have been built to study DM through electron recoils instead. As the electron is 4 orders of magnitude lighter than the nucleus, electron recoils can be induced by DM down to 4 orders of magnitude lighter than the lightest DM particle probeable with nuclear recoils.

In order to understand current and upcoming results from experiments searching for DM induced electron recoils, a theoretical understanding of DM electron scatterings in detector materials is needed. This requires input both from dark matter and material physics, and so far DM electron interactions have only been studied within the dark photon model. In the dark photon model, the DM-electron scattering takes a relatively simple form, and the material responds to the scattering through a single "response function".

Relaxing the assumption of the dark photon model, and instead applying Non-Relativistic Effective Theory approach, we calculate the expected detector signature for a wide range of DM models in Silicon and Germanium. In the papers of this thesis, we find that in contrast to the single response function produced by the dark photon model, the material can respond with 7 different response functions. These novel response functions we show to generically arise in a wide range of DM-electron interactions. As such, the papers of this thesis vastly extends the forms of DM-electron interactions that can be studied in Silicon and Germanium based experiments. These interactions made studyable by the works underlying this thesis are not fringe cases, but generically arise in a wide range of models. To illustrate this we consider a range of simplified models with a DM particle with spin 0, spin 1/2 and spin 1.

Keywords: Dark matter, direct detection, effective theory

To Jasmina.

List of Publications

Publications Included in this Thesis

1. R. Catena, T. Emken, M. Matas, N. A. Spaldin, and E. Urdshals, "Crystal responses to general dark matter-electron interactions," *Phys. Rev. Res.*, vol. 3, no. 3, p. 033 149, 2021

2. R. Catena, D. Cole, T. Emken, M. Matas, N. Spaldin, W. Tarantino, and E. Urdshals, "Dark matter - electron interactions in materials beyond the dark photon model," Oct. 2022, arXiv: 2210.07305

Other Publications not Included in this Thesis

F. Kahlhoefer and E. Urdshals, "On dark atoms, massive dark photons and millicharged sub-components," *Phys. Lett. B*, vol. 807, p. 135 601, 2020

Statement of Contributions

1. In Paper 1, I developed most of the theoretical framework, developed the code and ran the numerical calculations and analysis, and wrote parts of the text.

2. In Paper 2, I provided support with using the code developed in Paper 1, and made figures 1 and 2.

Acknowledgments

I would like to thank Riccardo Catena for his careful and detailed supervison. Your door is always open, and I have truly learned a lot from our many physics discussions. Your width of knowledge never cease to amaze me.

I would also like to thank my until recently co-supervisor Timon Emken for many fruitful discussions. Your rigour and attention to details has thought me a lot, and helped caution me against jumping to conclusions.

To Daniel, Nicola, Marek and Luca: Thank you for your fruitful collaboration. Daniel for his quick understanding and thorough work on the physics of dark matter electron interactions, and Nicola, Marek and Luca for teaching me a lot from you about the amazing physics of solids and fluids from you, a field I had little experience with before starting my PhD.

Acronyms

ALP:	Axion Like Particle
CMB:	Cosmic Microwave Background
CP:	Charge-conjugation Parity
DD:	Direct Detection
DFT:	Density Functional Theory
DM:	Dark Matter
EFT:	Effective Field Theory
GGA:	Generalized Gradient Approximation
GW:	Gravitational Waves
LSD:	Local Spin Density
LSS:	Large Scale Structure
NR-EFT:	Non-Relativistic Effective Field Theory

PBH:	Primordial Black Hole
QCD:	Quantum Chromodynamics
QFT:	Quantum Field Theory
SD:	Spin Dependent
SHM:	Standard Halo Model
SI:	Spin Independent
SM:	Standard model
WIMP:	Weakly Interacting Massive Particle

Contents

Part I

Overview

CHAPTER 1

Introduction

In modern physics, the mystery of dark matter (DM) is one of the most fundamental and fascinating problems yet to be solved. On the one hand the effects of the gravitational pull of DM on visible matter such as electrons and protons in the universe implies that DM makes up 85% of the matter content of the universe [1]. On the other it is still unknown what DM is made of.

The gravitational effects of DM are seen on several scales, and play a crucial role in understanding the universe. Shortly after the Big Bang, visible matter is being kept from clumping due to the photon radiation pressure. In contrast, a defining feature of DM is that it couples weakly to the photon, and is therefore free to clump together and form gravitational wells that pull on the visible matter[1]. These wells give rise to over- and underdensities of visible matter, which has been observed in the cosmic microwave background by WMAP [2] and Planck [3]. The gravitational wells formed by DM do not only play a role in shaping the cosmic microwave background; they are also crucial in structure formation, the process in which cosmological structures such as galaxies form around these gravitational wells. Both the origin of the

[1] In fact the visible matter density oscillates around these wells, a phenomenon called Barion Acoustic Oscillations.

cosmic microwave background and the structure formation of galaxies is well described and understood by the ΛCDM[2] model, also known as the Standard Model of Cosmology. The success of ΛCDM, a model in which DM is a key component, is strong evidence of the existence of DM.

The gravitational effect of DM is not only seen on cosmological scales, but also on the scales of galaxy clusters, galaxies and dwarf galaxies. It was first observed on these scales through the comparison of the velocity dispersion of the galaxies in the Coma cluster with the visible mass contained in the stars in these galaxies. The comparison showed that there had to be invisible dark matter in addition to the glowing stars in order to provide enough gravitational pull to produce the observed velocities [4]. Later, one has more systematically mapped velocities of stars and other visible objects such as hydrogen clouds as a function of distance from the center of galaxies in what is known as galactic rotation curves[3]. Today, rotation curves are used to infer DM density distributions in galaxies, information which is a valuable input in experiments to detect DM, and which is used to obtain the results in the papers on which this thesis builds.

There is a large number of candidates for DM. A notable one is primordial black holes (PBH) [5]; black holes formed in the early universe which remain until today. This is an attractive candidate as it does not require new physics. Within general relativity, PBH can be formed as a result of over densities in the early universe, and would survive until today as long as the mass is larger than $10^{15}\,\mathrm{g}$[4]. There are however multiple expected effects of PBH, such as destruction of neutron- and dwarf stars and lensing effects of PBH passing between Earth and distant stars which one does not observe. Due to this lack of observation it now seems unlikely that PBH can constitute all of DM [8], although it is still possible that PBH can make up some of the DM. This possibility will be further clarified by the recent breakthrough in observations of gravitational waves (GW) by the Ligo and Virgo collaborations [9], and

[2] Λ here refers to the cosmological constant, whereas CDM stands for Cold Dark Matter. These are the two ingredients that need to be added to standard particle physics and general relativity to correctly predict the cosmic microwave background and the details of structure formation.

[3] Galactic rotation curves are plots of the velocity of visible objects such as stars, and more recently hydrogen clouds, as a function of their distance to the center of the galaxy. From this the mass distribution within the galaxy can be inferred.

[4] Black holes evaporate due to Hawking radiation [6], [7], and the lower mass limit of $10^{15}\,\mathrm{g}$ is easily obtained knowing the physics of Hawking radiation and the age of the universe. It is stated in ref. [5], published the year after the first publication on Hawking radiation.

upcoming experiments are expected to measure GW with even greater sensitivity. They would be able to detect GW emitted from mergings of PBH with each other or with compact objects such as neutron stars, thereby shedding more light on a possible population of PBH.

Another possibility[5] is that DM is made up of particles, which will be the underlying hypothesis of this thesis. As there is no particle in the Standard Model of Particle Physics (SM) that can constitute DM[6], new physics is needed and the number of proposed models of DM particles is vast. The most popular is the Weakly Interacting Massive Particle (WIMP), a massive particle which interacts with the SM via the weak force. The reason for the popularity of WIMPs is (in addition to its simplicity) the so called WIMP miracle; the annihilation cross section needed to create the measured amount of DM from equilibrium with the SM particles in the early universe, is comparable with that of the weak interaction. This mechanism of DM creation is known as the freeze-out mechanism[7], as the DM particles are in equilibrium with the SM particles while the universe is sufficiently dense and warm, before leaving equilibrium (freezing out) as the universe expands and cools down at a rate larger than the WIMP annihilation rate.

The axion is another popular DM candidate, a particle which was initially introduced to solve a different problem in particle physics, namely the strong CP problem[8]; Quantum Chromo Dynamics (QCD) seems to be accidentally symmetric under simultaneous charge-conjugation (C) and parity (P) transformations. A proposed explanation for this symmetry is that the CP symmetry corresponds to the ground state of a new field [11], [12], which was later realised to correspond to a new particle with the properties of DM [13], [14].

The sterile neutrino [15] is yet another DM candidate with the added ben-

[5] A third possible explanation of the phenomena typically explained by DM is Modified Newtonian Dynamics[10], in which the Newtonian laws of motion are modified to fit galactic rotation curves.

[6] There is no standard model particle which both has a life-time longer than the age of the universe, interacts weakly enough with light and is heavy enough that it can form the gravitational wells in the early universe.

[7] Another popular and more recently proposed mechanism for DM production in the early universe is known as freeze-in. In this scenario DM never interacts strongly enough with the SM particles for it to be in equilibrium with the SM, but it still interacts strongly enough with the SM that energy leaks from the thermal bath of the SM into that of DM.

[8] In fact the name axion comes from a laundry detergent, since the axion was introduced to clean up the strong CP problem.

efit of solving an additional problem in physics, namely the neutrino mass problem; in the SM neutrinos are massless particles, but phenomena such as neutrino oscillation [16], [17] require the neutrino to have a small, but non-zero mass. This small neutrino mass can be explained by the seesaw mechanism by which the smallness of the neutrino mass is the consequence of the comparatively large mass of the hypothesized sterile neutrino [18].

The candidates for particle DM mentioned above have in common that they interact with each other and the particles of the SM not just gravitationally, but also through other forces. In fact, DM self-interaction might alter the DM distribution in galaxies by DM particles colliding and forming a core in contrast to the cusp like profile expected from non-interacting DM. The DM density profiles expected from self-interaction seem to fit observations better than the ones expected from collisionless DM [19], [20], suggesting DM indeed has non-gravitational interactions and motivating experiments to detect them.

Numerous experiments have been carried out to observe these hypothesised non-gravitational DM interactions with the SM. These experiments fall into 3 categories. The first is that of indirect detection experiments. Several DM models, such as the WIMPs, have the feature that pairs of them can annihilate into highly energetic SM particles. If this happens in or near our galaxy, these SM particles might reach earth and be detected. There is a wide range of experiments searching for such particles. Experiments such as DAMPE, Fermi-LAT, H.E.S.S. search for gamma rays [21]–[23] and cosmic rays[9] [24]–[26], whereas other are dedicated gamma ray experiments such as MAGIC [27] and VERITAS [28], or cosmic ray experiments such as AMS-02 [29]. In addition to gamma rays and cosmic rays there are also experiments searching for neutrinos, such as IceCube [30], ANTARES [31] and KM3NET [32]. These search for neutrinos interacting with water molecules, the first in the Antarctic ice, and latter two in the sea.

Another category is that of particle collider experiments, which work on the opposite principle of the indirect detection experiments. Rather than having DM particles annihilate into SM particles, one accelerates SM particles to very high energies and collide them to produce new particles, hoping some of them might be candidates for DM. In these experiments one looks for missing transverse momentum, i.e. missing momentum carried away by DM particles

[9] Cosmic rays are highly energetic charged particles such as electrons, protons and their anti particles.

after the momentum of all the detectable SM particles has been accounted for. The most notable of these particle colliders is the LHC. It accelerates protons to energies of several TeV, which lead to the discovery of the Higgs boson in 2012 [33]–[35]. Other examples include the Tevatron, known for discovering the top quark [36]–[38], and Belle[10] [39].

The third category is that of direct detection (DD) experiments, the experimental category this thesis will focus on. Such experiments search for energy and momentum deposited by DM in detector materials on earth. Compared to the method of indirect detection mentioned above, DD has the advantage that the interaction between DM and visible matter happens in the lab on earth. This makes it easier to control the environment in which the physics happens and reducing uncertainties from the DM density profile along the line of sight, and from the propagation of charged annihilation products in the galactic magnetic field. The observable deposition of energy and momentum can either happen through absorption of the DM particle, i.e. the mass energy of the DM particle is deposited in the detector, or through elastic scattering, i.e. (parts of) the kinetic energy of the DM particle is deposited. Detection of axions fall in the former category, whereas WIMPs and sterile neutrinos fall in the latter. So far the direct detection community has mostly focused on the detection of WIMPs, and designed experiments with this purpose. WIMPs are expected to have a mass range suitable for depositing energy to nucleus[11], causing the nucleus to recoil. Several experiments are built to search for these nuclear recoils, and their characteristics depend on whether they use solid or liquid detector materials. The liquid detectors mostly use noble gasses such as liquid xenon for XENON1T [41], XENONnT [42], LUX [43] and LZ [44], and liquid argon for Darkside50 [45] and DEAP-3600 [46]. The advantage of liquid detector materials is that they are easy to scale up, allowing experiments with tons of detector material.

Solid target experiments, on the other hand, operate various crystals as detector materials and are much smaller than their liquid counterparts, with typical masses ranging from grams to a few kilograms. They do however operate with a smaller energy threshold, making them better suited to probe

[10] Unlike LHC and Tevatron which collides protons with each other, Belle collides electrons with positrons.

[11] The WIMP mass is expected to range from 2 GeV to 100 TeV [40], and for kinematical reasons energy transfer in elastic scatterings lose efficiency when the DM mass differs from the target mass. Considered target masses range from light nucleus like that of oxygen with a mass of 16 GeV to 134 GeV for xenon nucleus.

lower DM masses. Notable experiments in this category are CRESST-III [47] using crystals of $CaWO_4$ as detector material, SENSEI [48] and DAMIC [49] using silicon crystals, EDELWEISS [50] using germanium crystals, and SuperCDMS [51] using both silicon and germanium crystals. Finally, there is a number of experiments using NaI crystals; COSINUS [52], ANAIS-112 [53] and DAMA [54]. The latter of these experiments report a scintillation signal with characteristics of DM induced nuclear recoils; it is reported to have the cosine shape with a maximum at June 2nd and minimum at December 2nd expected from yearly modulation[12]. As such, DAMA reports to be seeing evidence of non-gravitational DM interaction, but the report of DAMA is controversial as none of the other above-mentioned collaborations see a similar signal[13].

As there is no decisive evidence for DM induced nuclear recoils, the DD community has started turning their attention towards DM induced electron recoils. Electrons have the advantage of being much lighter than the nucleus, and are therefore suitable for probing much lower DM masses[14] than what is feasible with nuclear recoils. If DM for example has a mass in the MeV-GeV range, electron recoil experiments might hold the key to the first direct detection of DM particles from our galaxy. An increased theoretical understanding of these DM induced electron recoils will be the main contribution of this thesis. Most of the above mentioned DD experiments, although tailored for nuclear recoils, are also sensitive to electron recoils. XENON1T did interestingly see an unexplained electron recoil spectrum [55] explainable with DM, although this has later been excluded by XENONnT [56], another xenon based experiment.

Other experiments are build with the purpose of detecting DM induced electron recoils. PTOLEMY [57], which uses graphene sheets as detector material, is such an experiment. In particular PTOLEMY is interesting as it measures electrons ejected from the graphene sheets, and from the direction of these electrons it can be (statistically) reconstructed from which direction the

[12] When the orbital velocity of Earth is maximally aligned with the velocity of the Sun relative to the galaxy, the velocity of Earth through the DM halo is at it's highest. At this time the incoming DM flux and velocity is maximal. Six months later the situation is the opposite and the DM flux and velocity is minimal. This modulation is useful as it allows for distinguishing DM signals from constant backgrounds.

[13] The purpose of ANAIS-112 and COSINUS is largely to crosscheck the result of DAMA with the same detector material to rule out effects from different detector materials.

[14] Electron recoils can be induced by DM masses down to the electron mass, i.e. $\sim 0.5\,\mathrm{MeV}$.

particle that caused the ejection came. Also, the probability of a DM particle ejecting an electron is highest for DM particles incoming perpendicular to the graphene sheet. As the DM flux reaching Earth is not isotropic but peaked in one direction, the rate of ejected electrons should vary throughout the day. This variation is called daily modulation, and helps to distinguish ejections caused by DM from other (constant) background sources.

In order to understand the DM induced electron recoils, modelling of DM interacting with electrons bound in materials is needed [58]–[62]. Since the non-gravitational interaction (if any) DM has with electrons is unknown, it is important to stay as general as possible. We model the interaction without making assumptions on its form for the first time by employing the framework of non-relativistic effective field theory (NR-EFT): It can be shown that for non-relativistic particles[15] all Galilean invariant interactions can be written in terms of a a finite number of effective operators [63]. The number of such operators is given as $4 + 20j_\chi$ [64], where j_χ is the spin of the DM particle. In practice, interactions described by all possible combinations of these effective operators need to be modelled in realistic detector materials. Focusing on the operators relevant to spin 0 and spin 1/2 DM, we do this for the first time for silicon and germanium crystals in Paper 1 using a state-of-the-art density functional theory (DFT) calculation to accurately capture the crystal physics. With the framework we develop and provide, the rate at which DM is expected to produce electron hole pairs in silicon and germanium crystals is easily computed. This expected rate allows for interpretation of the data from experiments such as SENSEI, SuperCDMS and EDELWEISS.

In Paper 2, we demonstrate the importance of the NR-EFT approach using the DFT calculation from Paper 1 together with results for atomic xenon from [65] to calculate the limits silicon, germanium and xenon based DD experiments place on a set of simplified models of DM. These models include scalar, vector and fermionic DM, and shows how one generically gets several contributing effective operators different from the operator usually studied in the benchmark model; the dark photon model. As we only consider simplified models, the number of operators for spin 1 are not 24, but rather 18.

These works, together with ref. [65], thus establish NR-EFT in the con-

[15] One of the few known properties of DM is that it is gravitiationally bound to the galaxy, and thus that it follows Keplerian motion with a velocity of $\sim 10^{-3}c$. The electron in the target material have a velocity of $\sim Z_{\text{eff}}\,\alpha$, and for the outermost electrons in an atom $Z_{\text{eff}} \sim 1$.

text of DM-electron scattering. It shows how going beyond the dark photon model generically reveals new physics with materials reacting in novel ways. As such, the works underpinning this thesis not only expands the DM model space that can be compared to experiments, but also unlocks novel material properties not probeable with the standard electromagnetic interactions typically considered.

CHAPTER 2

Evidence for dark matter

Dark Matter (DM) is a key ingredient in cosmology as well as well as galactic and extragalactic astrophysics. In this chapter these topics will be reviewed with an emphasis on the aspects relevant to DM.

2.1 Cosmology

In the beginning the inflaton created a thermal bath of particles. Now the bath was formless (homogeneous) with the exception of some very small density perturbations.

Below, the evidence for DM will be discussed on cosmological scales. These are scales larger than galaxy clusters. First, a review of the Standard Model of Cosmology will be given, in which the abundance of dark matter is a free parameter. We will then see that the value of this parameter can be inferred by comparing measurements of the Cosmic Microwave Background (CMB) with simulations based on general relativity and hydrodynamics. Finally, Large Scale Structure (LSS) formation will be discussed.

The Standard Model of Cosmology

The Friedmann model describes an expanding homogeneous universe. It is given by the FLRW[1] metric

$$\mathrm{d}s^2 = -\mathrm{d}t^2 + a^2(t)\left[\frac{\mathrm{d}r^2}{1-kr^2} + r^2\left(\mathrm{d}\theta^2 + \sin^2\theta\,\mathrm{d}\phi^2\right)\right], \tag{2.1}$$

where k is the spatial curvature parameter, and equals 0 for a flat universe. t is the cosmological time, i.e. the time of an observer who sees the universe as being homogeneous[2]. r, θ and ϕ are the spherical comoving coordinates, meaning that they are constant in time and do not expand together with the universe. The time dependence is absorbed in $a(t)$, the scale factor, which increases with time as the universe expands. The Friedmann law can be derived from the Einstein equation, and it governs the time evolution of a:

$$H^2 \equiv \left(\frac{\dot{a}(t)}{a(t)}\right)^2 = \frac{8\pi G}{3}\rho - \frac{k}{a^2} + \frac{\Lambda}{3}, \tag{2.2}$$

with H being the Hubble rate, ρ being the energy density and Λ being the cosmological constant. From the Bianchi identities it can be shown that energy conservation demands that

$$\dot{\rho} = -3\frac{\dot{a}}{a}(\rho + p), \tag{2.3}$$

with p being the pressure. This relation holds for the total energy of the universe, and for decoupled species. One can distinguish between radiation (here taken to be any particle for which $E \gg m$, with E being the energy of the particle and m being the mass) and matter (here taken to be any particle for which $E \approx m$). Matter is pressureless ($p \approx 0$) and radiation has a pressure of $p \approx \frac{\rho}{3}$. From the above energy conservation equation it then follows that

$$\rho_m \propto a^{-3}, \qquad \rho_r \propto a^{-4}, \tag{2.4}$$

[1] The metric is named after Alexander Friedmann, Georges Lemaître, Howard P. Robertson, and Arthur Geoffrey Walker.

[2] The frame in which the universe is homogeneous is the frame in which the cosmic fluid is at rest.

where ρ_m is the density of matter and ρ_r is the density of radiation, with the total density $\rho = \rho_m + \rho_r$. This result can be intuitively understood; The volume of the universe grows as a^3, and for a fixed number of matter particles in a changing volume the density is inversely proportional to the volume. Radiation also gets diluted by the increasing volume just like the matter particles, and in addition it gets red-shifted. As radiation energy is inversely proportional to the wave-length, and the wave-length increases proportionally to a, the radiation volume gets diluted with an additional a^{-1}.

The Friedmann Law thus contains terms proportional to a^{-4} (radiation), a^{-3} (matter), a^{-2} (curvature) and a^0 (cosmological constant Λ), each of which can dominate for different values of a. For small a one can have radiation domination, then matter domination, then curvature domination and finally Λ domination. To make this clearer the concept of critical densities can be introduced;

$$\rho_c \equiv \frac{3H^2}{8\pi G}\,, \qquad\qquad \rho_c^0 \equiv \frac{3H_0^2}{8\pi G}\,, \tag{2.5}$$

with ρ_c being the critical density and ρ_c^0 (H_0) being the critical density (Hubble rate) today. From this the Ω parameters can be defined:

$$\begin{aligned} \Omega_m &\equiv \frac{\rho_m^0}{\rho_c^0} = \frac{\rho_b^0}{\rho_c^0} + \frac{\rho_{\rm DM}^0}{\rho_c^0} \equiv \Omega_b + \Omega_{\rm DM}\,, \\ \Omega_r &\equiv \frac{\rho_r^0}{\rho_c^0}\,, \quad \Omega_k \equiv \frac{-k}{a_0^2 H_0^2}\,, \quad \Omega_\Lambda \equiv \frac{\Lambda}{3H_0^2}\,, \end{aligned} \tag{2.6}$$

with a_0, ρ_b^0 and $\rho_{\rm DM}^0$ being the value of a and the density of baryons[3] and DM today respectively. Inserting this in eq. (2.2), it becomes

$$\frac{H^2}{H_0^2} = \left[\Omega_r \left(\frac{a_0}{a}\right)^4 + \Omega_m \left(\frac{a_0}{a}\right)^3 + \Omega_k \left(\frac{a_0}{a}\right)^2 + \Omega_\Lambda\right]\,, \tag{2.7}$$

$$\frac{H^2}{H_0^2} = \left[\Omega_r \left(1+z\right)^4 + \Omega_m \left(1+z\right)^3 + \Omega_k \left(1+z\right)^2 + \Omega_\Lambda\right]\,, \tag{2.8}$$

where z is the cosmological redshift, i.e. the redshift of photons between t and today due to the expansion of the universe. Today $H = H_0$, $a = a_0$ and

[3]The mass density of electrons is negligible.

$z = 0$, so the Friedmann equation reads

$$1 = \Omega_r + \Omega_m + \Omega_k + \Omega_\Lambda \,. \tag{2.9}$$

As such Ω_i can be interpreted as the fractions of the total energy of the universe in form i, and the above equation is often referred to as the budget equation.

Cosmic Microwave Background

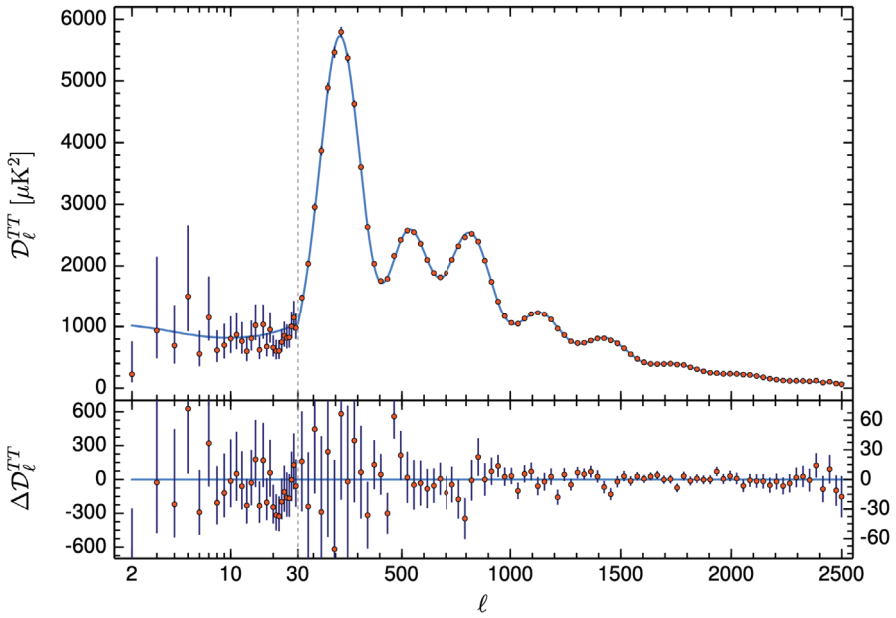

Figure 2.1: The CMB power spectrum taken from Planck 2018 [1]. The blue line is the theoretical prediction from ΛCDM with the cosmological parameters given in eq. (2.11), and the red dots are the values inferred from the measurements of the CMB with 1σ error bars. The upper panel shows the spectrum, whereas the lower panel shows the discrepancy between the theoretical prediction and the measured result. Note that the horizontal scale changes from logaritmic to linear at the vertical dashed line at $\ell = 30$, and that also the vertical plot range in the lower panel is reduced by a factor of 10 to the right of the line.

When the universe is warm, with a temperature larger than the ionization energy of hydrogen, the baryons and electrons in the universe constitute a plasma through which photons do not propagate freely. As it cools down to

a temperature of around 0.26 eV the electrons recombine with the protons to form neutral hydrogen, allowing the thermal photons to propagate freely. These photons then travel through the expanding universe, get red-shifted by a factor of $z_* = 1090$, and arrive at earth from all directions (i.e. their origin is described by two angles) with a temperature of 2.3×10^{-4} eV. They have the spectrum of a black body, and the temperature of photons coming from different directions have small relative variations[4] of 10^{-5}. These variations can be described by a multipole expansion[5] with coefficients $\mathcal{D}_\ell^{TT}$ shown in fig. 2.1 and defined as [3]

$$\begin{aligned} \mathcal{D}_\ell^{TT} &= \sum_m \frac{\ell(\ell+1)}{2\pi} \left\langle a_{\ell m}^{T*} a_{\ell m}^{T} \right\rangle , \\ a_{\ell m}^{T} &= \int \mathrm{d}\,\hat{\mathbf{n}}\, Y_{\ell m}^{*}\left(\hat{\mathbf{n}}\right) \delta T\left(\hat{\mathbf{n}}\right) , \end{aligned} \tag{2.10}$$

with $\delta T\left(\hat{\mathbf{n}}\right)$ being the temperature perturbation of the CMB photons coming from direction $\hat{\mathbf{n}}$, and $Y_{\ell m}$ are spherical harmonics. $\langle\rangle$ refers to the average over the temperature perturbations simulated with different initial conditions for the density distribution of the universe. These are typically assumed to be Gaussian distributed, and the expected distribution of $\delta T\left(\hat{\mathbf{n}}\right)$ is simulated from the Einstein equations and hydrodynamical equations.

$\delta T\left(\hat{\mathbf{n}}\right)$ is also inferred from measurements of the photon temperature of the CMB, and the averaging $\langle\rangle$ is done over different patches of the sky. For small ℓ there are few sky patches to average over, causing the error bars to be large. Comparing the measurements to the simulations one infer the values of the parameters in the ΛCDM that cause the simulations to fit the measurements.

The effect of DM is intuitively understood, as DM can clump together much more efficiently than baryons. This is due to DM not feeling the radiation pressure of the photons. It then forms gravitational wells around which the baryons oscillate in what is called baryon acoustic oscillations. In particular,

[4] Somewhat counter intuitively, the regions of the sky that appear the warmest are in fact the coldest. This is known as the integrated Sachs-Wolfe effect [66], and is due to warmer regions having higher mass densities, causing the photons to get more gravitationally red-shifted as they propagate towards Earth, an effect which is stronger than the initial higher temperature of the photons emitted from these regions.

[5] In fact, the by far strongest variation comes from the motion of the earth relative to the cosmic rest frame (the frame in which the CMB is the most isotropic). This is Doppler shift is being subtracted from the measured CMB to obtain the distribution one would have seen if the earth was in the cosmic rest frame.

the absence of DM would suppress the second peak in fig. 2.1. As such, DM is vital in forming the CMB, and from fig. 2.1 one sees that there is excellent agreement between the prediction of the ΛCDM shown in the blue line and the measurement shown with the red dots.

These best fit values of Ω_r, Ω_m, Ω_k, Ω_Λ, Ω_b and Ω_{DM} producing the blue line in fig. 2.1 are not only fit to the CMB but also to other measurements. They are [1]

$$\begin{aligned} \Omega_m &= 0.3111\,, \quad \Omega_b = 0.0492\,, \quad \Omega_{\mathrm{DM}} = 0.2630\,, \\ \Omega_r &= 0.0001\,, \quad \Omega_k = 0.0007\,, \quad \Omega_\Lambda = 0.6889\,, \end{aligned} \tag{2.11}$$

from which one sees that DM makes up 26.3% of the energy content and 84.5% of the matter content of the universe. Note that $\Omega_m \gg \Omega_k$ and $\Omega_\Lambda \gg \Omega_k$, so there is no time (no value of $z > 0$) at which the term proportional to Ω_k dominates the right hand side of eq. (2.8). In fact, the measured value of Ω_k is compatible with 0 and usually neglected. The curvature being negligible is typically explained with inflation, in which the early universe goes through an accelerating expansion, flattening out any initial curvature.

Large Scale Structure

ΛCDM does not only explain the CMB; it also describes how the clumping of DM that give rise to the CMB goes on to form large scale structures (LSS), structures larger than $\sim 100\,\mathrm{Mpc}$. Without DM, the structures could not have started forming until the universe became transparent to electromagnetic radiation at the time of recombination. These theoretical descriptions of LSS formation are typically obtained by N-body simulations with the density perturbations from the CMB as initial conditions, in which the dynamics of the mass over densities due to DM at the time of recombination is evolved to simulate the mass density distribution today. The density distribution can be compared to observations of the large scale structures [68] such as galaxies and galaxy clusters to find excellent statistical agreement [69]. This agreement is examplified in fig. 2.2 where the observed galaxy distribution is shown in blue and the simulated galaxy distribution obtained with ΛCDM is shown in red.

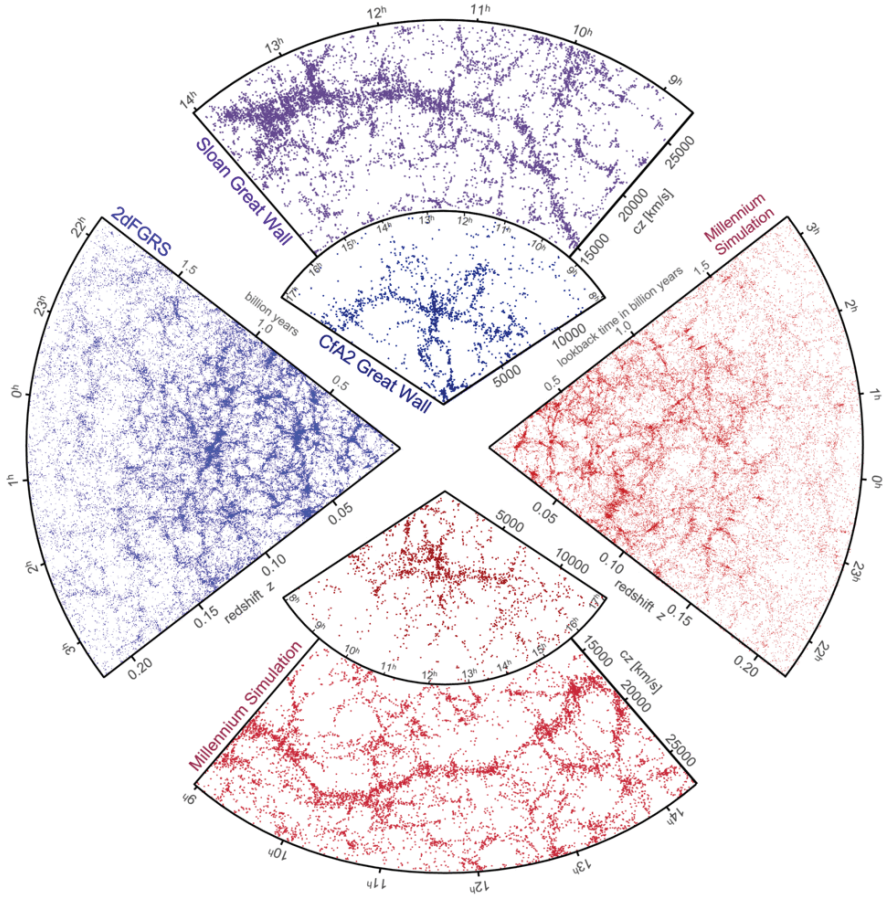

Figure 2.2: A comparison between observed galaxy distribution (blue) and simulated galaxy distribution (red) taken from [67].

2.2 Astrophysics

The gravitational effects of DM is not only seen on cosmological scales, but also in astrophysical scales such as galaxy clusters, galaxies and dwarf galaxies. DM is needed to explain their formation, and the gravitational mass is measured to be much larger than the visible mass. These measurements of the gravitational mass are done with multiple methods. Two of these, weak lensing and galactic rotation curves will here briefely be discussed.

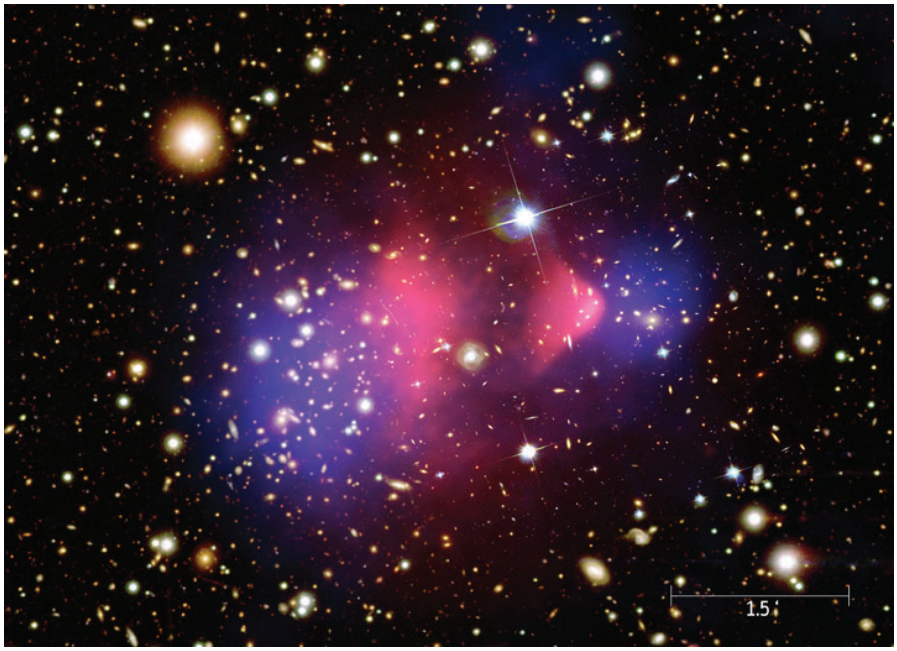

Figure 2.3: Image of the Bullet Cluster showing gravitational lensing in blue [70], x-ray radiation in red [71] together with the optical image [72].

Weak gravitational lensing

General relativity [73] describes how massive objects bend the trajectory of light, a phenomenon known as gravitational lensing. Large astrophysical objects such as galaxy clusters create a measurable lensing effect, which in turn can be used to infer the gravitational mass of the astrophysical object. One generally distinguishes between strong and weak lensing. By strong lensing one refers to gravitational lensing strong enough to produce multiple images around a massive object. This is due to the photons being "caught" and orbiting multiple times around the massive object before escaping. Weak lensing, on the other hand, causes small distortions of the original image, and from these distortions one can statistically infer the mass density that caused the distortions.

This is done for the Bullet Cluster in fig. 2.3. The image shows two galaxy clusters that are colliding, and the blue color shows the mass density infered from gravitational lensing whereas the red color shows the x-ray density. As the x-rays mostly come from the hydrogen gas that makes up most of the visible mass of the galaxy, the red color shows the density of visible mass

whereas the blue color shows the density of total mass. As is evident from the image, the hydrogen clouds collide with each other and lose some of their velocity, whereas the clouds of dark matter pass through each other largely unaffected. This is a strong indicator of the present of a large invisible mass that interacts weakly enough with itself and with the visible matter that it does not cause sizeable friction.

Galactic rotation curves

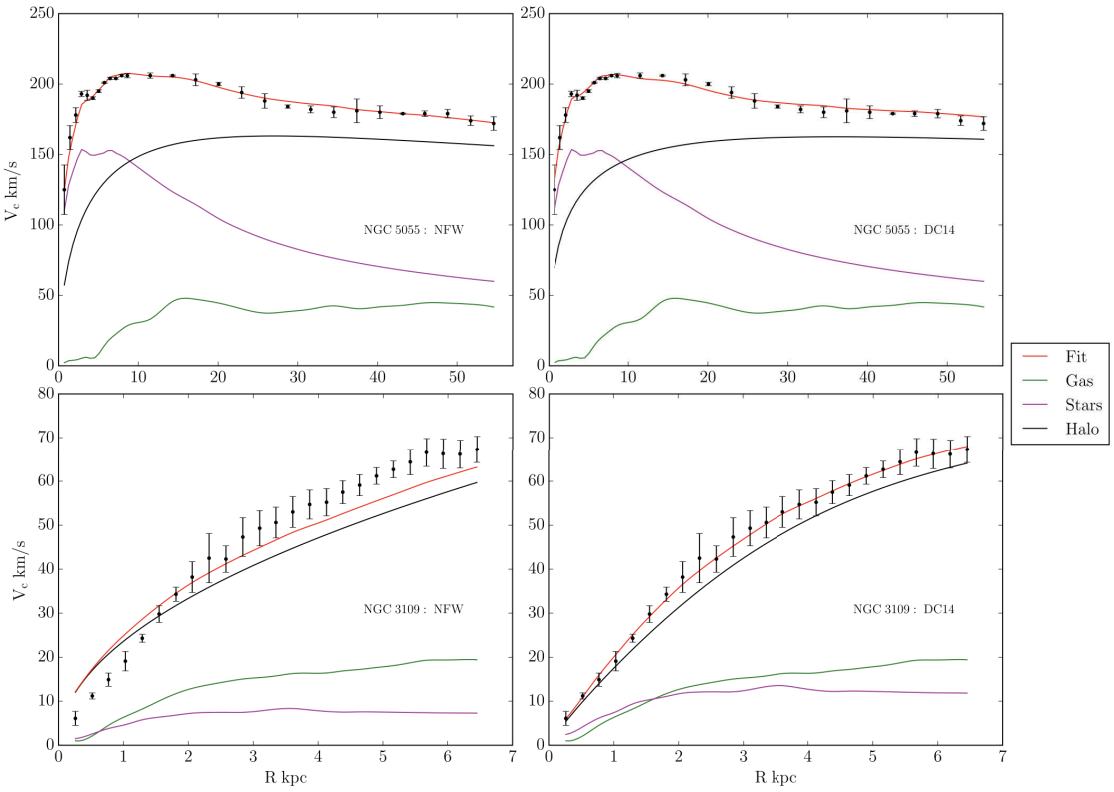

Figure 2.4: Plot by ref. [74] showing measured velocity distribution of visible objects in galaxies as function of distance from the galactic center. The pink and green lines shows the contribution to the velocity distribution from the stars and gas clouds in the galaxy, respectively, whereas the black line shows the best fit DM distribution obtained with the NFW method in the panels to the left and the DC14 method in the panels to the right. Together these contributions produce the red line. The upper two panels are for a galaxy with a large mass, whereas the lower panels are for a galaxy with a smaller mass.

The discrepancy between the gravitational mass and the visible mass was first observed in the 1930s by Zwicky and Smith. They compared the velocity of galaxies with the visible mass in the Coma and Virgo clusters respectively [75], [76], and found a discrepancy Zwicky referred to as dark matter[6]. The circular velocity v of a gravitationaly bound object is given from Newtonian physics [77] as[7]

$$v(r) = \sqrt{4\pi r \int_0^r \mathrm{d}\tilde{r}\, \rho(\tilde{r})}\,, \tag{2.12}$$

so the distribution of the mass density of the galaxy, ρ, can be inferred by measuring $v(r)$ for multiple r. These measurements of $v(r)$ are shown in fig. 2.4. There the expected velocity distributions from the mass density of the observed gas, the observed stars and best fit DM halo is shown with the green, pink, and black line respectively. Combined they form the red line as the predicted total velocity.

[6] Zwicky was however not the first who used the term dark matter to refer to invisible matter in the universe. See [4] for details on the history of dark matter.

[7] For simplicity ρ is here taken to be spherically symmetric, an approximation which is not as bad as it might seem as most of the mass of galaxies is believed to lie in a dark matter halo rather than in the stellar disk.

CHAPTER 3

Particle Dark Matter

In chapter 2 we saw that measurements of the CMB together with other astrophysical sources show that DM makes up 84.5% of the matter content of the universe, but these measurements do not give information of the underlying structure of DM[1]. There have been suggested several models to account for this invisible mass, ranging from massive objects such as primordial black holes to elementary particles or composites thereof. In this thesis DM is assumed to be particles described by Quantum Field Theory (QFT). From a Direct Detection (DD) perspective one can divide DM models into two classes; DM particles that scatters elastically with SM particles depositing parts of its kinetic energy to the SM particles; and DM particles that can be absorbed by SM particles, depositing its entire mass-energy. These two classes of DM models will be discussed briefly below, before mechanisms by which it can be created will be discussed.

[1] It should be noted that the similarity between the abundance of DM and SM particles suggest that they might have a common origin and therefore have some form of interaction. This common origin would also indicate that the DM and SM particles should have similar masses, i.e. that the DM particle should have a mass in the meV to TeV range, much of which is probeable with direct detection experiments.

3.1 A selection of DM models

WIMPs and sub-GeV DM

WIMPs are stable Weakly Interacting Massive Particles interacting with the standard model through the weak force. WIMPs are highly motivated from the WIMP miracle mentioned in the introduction, and particles with the properties of WIMPs naturally arise in models such as Supersymmetry. In order for enough of them to be produced via the freeze-out mechanism to be discussed later in this chapter they need to have a mass larger than about 2 GeV [40]. They serve as the benchmark model for most DD experiments. With the lack of detection of such particles however, several models of lighter sub-GeV DM have also been proposed. These would be too light to induce detectable nuclear recoils. What these models have in common is that they feature a stable DM particle which couples to the SM via a mediator lighter than the gague bosons mediating the weak force. The lighter mediator relaxes the lower bound on the WIMP mass of 2 GeV for production via freeze out. These particles can scatter elastically with SM particles, transferring (a fraction of) its kinetic energy to the SM particle. As such, from a DD perspective these models can be characterized by the mass of the DM particle and the nature of its interaction with the SM. The most popular (and simplest) of these is the dark photon model.

Dark photon model

The dark photon model extends the standard model with an additional $U(1)$ gauge group with which the dark photon A'_μ is the associated gauge boson. The DM particle χ couples to the dark photon in the same way as the photon couples to charged particles in the SM. Furthermore this dark photon is usually taken to kinetically mix with the SM photon, giving rise to interactions between DM and ordinary charged matter. In this model, the dark sector is described by the Lagrangian

$$\mathscr{L}_D = \bar{\chi}(i\gamma^\mu D_\mu - m_\chi)\chi + \frac{1}{4}F'_{\mu\nu}F'^{\mu\nu} + m^2_{A'}A'_\mu A'^\mu + \varepsilon F_{\mu\nu}F'^{\mu\nu}\,, \qquad (3.1)$$

with the covariant derivative defined as

$$D_\mu \chi = \partial_\mu \chi - i g_D A'_\mu \chi \,, \tag{3.2}$$

where g_D is the gauge coupling corresponding to the dark $U(1)$ gauge group, $F'^{\mu\nu}$ is the dark photon field strength tensor, $m_{A'}$ is the dark photon mass and ϵ is the kinetic mixing strength. This model has the advantage that the dark photon behaves like the SM one, which is well understood and leads to a simple expression for the DM-SM scattering cross section. The above Lagrangian is for a spin 1/2 DM particle, but DM particles with other spins are also extensively studied in the literature.

Other non-standard interactions

Using the dark photon model as a benchmark might however cause one to miss potential signatures of DM caused by other more complicated interactions. Covering all possible interactions DM can have with SM requires Effective Field Theory (EFT) approaches, discussed in the context of direct detection of DM-electron interactions in section 4.3. It can however be illustrative considering a few non-standard interactions DM can have with SM to show how their signatures differ from that of the dark photon model. In Paper 1 non-standard interactions are considered to illustrate potential deviations from the phenomenology of the dark photon model [65], [78]. Dark matter could interact with the photon field through an electric dipole moment,

$$\mathscr{L}_{\text{int}} = \frac{g}{\Lambda}\, i\bar{\chi}\sigma^{\mu\nu}\gamma^5\chi\, F_{\mu\nu} \,, \tag{3.3a}$$

where g is the coupling strength and Λ is the energy scale at which the electric dipole is generated. Likewise, the DM particle can have a non-zero magnetic dipole moment described by the Lagrangian interaction term

$$\mathscr{L}_{\text{int}} = \frac{g}{\Lambda}\, \bar{\chi}\sigma^{\mu\nu}\chi\, F_{\mu\nu} \,, \tag{3.3b}$$

where again g and Λ are the coupling and the energy scale at which the magnetic dipole is generated, respectively. Dark matter might also interact

through the anapole interaction,

$$\mathscr{L}_{\rm int} = \frac{g}{2\Lambda^2}\,\bar{\chi}\gamma^\mu\gamma^5\chi\,\partial^\nu F_{\mu\nu}\,. \tag{3.3c}$$

In Paper 1, effective field theory is used to calculate the rate at which DM with these interactions scatters off bound electrons leaving observable signatures in direct detection experiments. In Paper 2 we go beyond the above mentioned non-standard interactions and look at generic DM-electron interactions for spin 0, spin 1/2 and spin 1 DM.

Axion and axion like particle dark matter

Axions and Axion Like Particles (ALPs) is a class of models for DM consisting of bosons with a mass of a few eV and below. The axion was originally proposed as a solution to the CP problem of QCD, in which QCD generically break CP symmetry via the Lagrangian term

$$\mathscr{L}_\theta = \overline{\theta}\frac{\alpha_s}{8\pi}G^{\mu\nu a}\tilde{G}^a_{\mu\nu}\,, \tag{3.4a}$$

with $G^{\mu\nu a}$ being the gluon field strength tensor and its dual being $\tilde{G}^{\mu\nu a} \equiv \epsilon^{\mu\nu\rho\sigma}G_{\rho\sigma}/2$. This term in the Lagrangian would generate an electric dipole moment for the neutron, the lack of observation of which requires $\overline{\theta} \lesssim 10^{-10}$ [79]. This required smallness of $\overline{\theta}$ is remarkable as $\overline{\theta}$ receive contributions from two independent quantities that happen to cancel almost exactly [80]. Known as the strong CP problem, the cancellation is popularly explained by the Peccei-Quinn mechanism [11], [12] in which the QCD axion field [13], [14], a, couples to the gluons via the Lagrangian term

$$\mathscr{L}_{\theta,a} = \left(\frac{a}{f_a} - \overline{\theta}\right)\frac{\alpha_s}{8\pi}G^{\mu\nu a}\tilde{G}^a_{\mu\nu}\,, \tag{3.4b}$$

with f_a being the axion decay constant. The ground state of the axion field corresponds to $a/f_a = \overline{\theta}$, eliminating the CP violating term [81]. The axion mass can be calculated with chiral perturbation theory to be [82]

$$m_a = \frac{f_\pi m_\pi}{f_a}\frac{\sqrt{m_u m_d}}{m_u + m_d} \approx \frac{10^{12}\,\text{GeV}}{f_a}\,5.691\,\mu\text{eV}\,, \tag{3.5}$$

with m_u, m_d and m_π being the masses of the up quark, down quark and pion respectively, and f_π being the pion decay width. The QCD axion mass is usually assumed to lie in the range $1\,\mu$eV to $100\,\mu$eV, as this is compatible with the axion being produced in an abundance matching that of DM.

Since the above described QCD axion was proposed, several other particles with similar characteristics referred to colloquially as ALPs have been proposed. These do not solve the strong CP problem and take m_a and f_a to be independent parameters. This allows for a much larger range of masses, $10^{-20}\,\text{eV} \lesssim m_a \lesssim \text{eV}$. Both axions and ALPs can oscillate into photons giving observable astrophysical signatures, or be absorbed in detectors on earth depositing their entire mass-energy to SM particle(s). For a review of axions and ALPs, see i.e. ref. [80], [83].

3.2 On The Origin of Dark Matter

There are several ways in which the DM particles can be created in the abundance matching the observed one. The abundance can be set by an asymmetry between the particle and anti-particle abundance [84] similar to the SM particles. DM can also be created from interactions with visible matter, through two mechanisms we discuss below; freeze out and freeze in.

Freeze Out

If the DM particles interact strongly enough with the SM particles to be in equilibrium with the thermal bath of SM, the abundance of DM is that for which the rate of annihilation matches that of creation[2]. As the universe expands, the density of both the SM particles and the DM particles is reduced, and so is the rate of annihilation and creation of DM particles. Furthermore, as discussed in the last section, the radiation in the thermal bath is red-shifted as the universe expands, causing the temperature to decrease.

As the temperature drops below the mass of the DM particles the creation rate becomes exponentially suppressed. For DM to remain in equilibrium with the SM particles the annihilation rate must also be exponentially suppressed, which in turn demands that the number of DM particles is exponentially

[2] Annihilation requires DM particles and anti-particles to collide, and this becomes more frequent the more DM particles and anti-particles there are. As such, the density of DM particles will naturally tend towards the equilibrium.

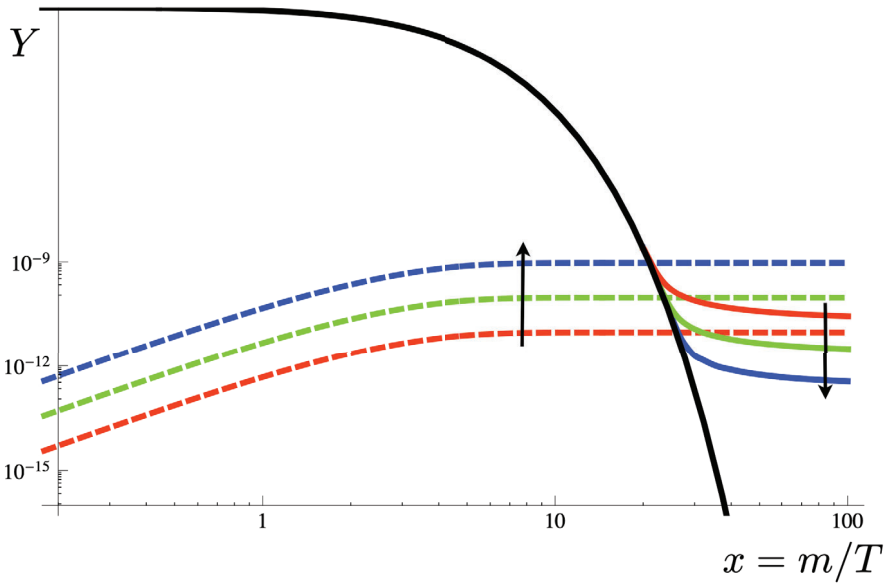

Figure 3.1: Illustrative plot of the freeze out mechanism (solid lines) and freeze in mechanism (dashed lines) from [85]. Y is the yield, and is proportional to the number of DM particles, whereas m here refers to the mass of the DM particle and T refers to the temperature of the SM bath. The black line shows the number of DM particles for DM in equilibrium, whereas the blue, green and red lines show the number of DM particles for different annihilation cross sections, with blue being the largest and red the smallest. The solid lines are for large enough annihilation cross sections that DM at high temperatures is in equilibrium with SM, whereas the dashed lines are for much smaller annihilation cross sections (but with the same relation between the colors) where DM never enters equilibrium with SM.

suppressed. This suppression can be seen in fig. 3.1 for $m_\chi/T = x > 1$, where m_χ is the mass of the DM particle and T is the temperature of the SM bath.

As both the rate of creation and annihilation drops, however, DM departs from equilibrium; it freezes out. It can be shown that DM particles on average interact less than once between the time at which the interaction rate equals the Hubble rate and today. The DM particles are therefore taken to be decoupled when this condition is met.[3] After DM is decoupled the number of DM particles remains fixed until today. The number of DM particles today is therefore determined by how much the number of DM particles is thermally suppressed before it leaves equilibrium (freezes out) [86], i.e. how long they

[3]It should be noted that even though DM has left chemical equilibrium it can still scatter elastically with the SM bath and thereby maintain kinetic equilibrium.

stay in equilibrium. The stronger DM interacts with the SM particles, the longer it stays in equilibrium and the fewer DM particles survives until today. This effect can be seen from the solid lines in fig. 3.1 where the red solid line departs from equilibrium (the black line) before the blue solid line, giving a higher value of Y, which is proportional to the number of DM particles in the universe.

Freeze In

An alternative to the freeze out mechanism is freeze in. In this scenario the creation and annihilation cross sections are never large enough for DM to be in equilibrium with the SM bath; the annihilation of DM into SM particles is negligible at all times, whereas DM is created from the SM bath until the rate of creation becomes thermally suppressed by the temperature dropping below the mass of the DM particle. This evolution of the number of DM particles is seen by the dashed lines in fig. 3.1, where the red line corresponds to a lower creation cross section and thus a lower number of DM particles than the green and blue lines.

It is worth stressing that the creation cross sections of the dashed colored lines are much smaller than the ones for the solid colored lines, and as such the two mechanisms for production of DM complement each other by covering different ranges of creation cross sections. As a final word on DM creation one can mention that the freeze in mechanism assumes that the initial number of DM particles is 0 (or at least very small), i.e. that whatever created the bath of SM particles did not also create a similarly large bath of DM particles. This assumption is not present in the freeze out regime, as a large initial DM bath would quickly annihilate into SM particles bringing the DM bath and the SM bath into equilibrium.

CHAPTER 4

Direct Detection of Dark Matter

As mentioned in the introduction, there are three main strategies for detection of DM. Collider searches involve accelerating SM particles to high energies and colliding them, causing the creation of additional particles. If DM is created, it will leave the detector undetected[1], carrying away momentum and energy. The detected particles will then seem to violate energy and momentum conservation, and from the missing energy-momentum one can conclude that undetectable particle(s) have been created. From the detected particles one can then reconstruct the interaction in which the DM was created[2].

Indirect detection experiments are searching for SM particles created by annihilating DM particles in space. If the DM particles have a mass similar to or larger than the massive SM particles it can annihilate into high energy SM particles, detected on earth as cosmic rays, gamma rays and neutrinos.

[1] There are also experiments attempting to detect high-velocity DM particles created from collisions of SM particles.

[2] This is similar to how the hints of the existence of the neutrino first emerged. It was noticed that electrons produced by beta decay took continuous energy values rather than the fixed energy of the nuclear transition. The existence of a neutral (and thus at the time not detectable) particle with which the electron share the energy from the nuclear transition was proposed and later detected.

As there also are other galactic sources of cosmic rays, the challenge is to distinguish cosmic rays due to DM from rays produced by other sources. Indirect detection can also be used to search for signals coming from models of lighter dark matter particles. Examples of this is impacts of axions on stellar physics and galactic gamma ray propagation, and radio flashes produced by axion condensates colliding with neutron stars.

Dark matter direct detection experiments are low background experiments searching for rare scattering events of DM with detector materials, where the DM deposits energy and momentum to the detector material. This deposited energy and momentum is then detected by means that vary between the experiments. In this chapter various direct detection experiments and techniques will be discussed. In the first section the density and velocity distribution of the DM near Earth will be covered, before the attention is moved to nuclear recoils in the second section. Finally, in the third section electron recoils are discussed in an EFT framework. The framework presented there is developed in the papers attached to this thesis.

4.1 Dark matter density in the milky way

The density and velocity distribution of DM is typically described by the so called Standard Halo Model (SHM). The velocity distribution is obtained by assuming that the DM particles are Boltzmann-distributed with the circular orbit velocity $v_0 = 238\,\mathrm{km/s}$ [87] being the most likely speed. Furthermore, the population of DM particles with velocities larger than the escape velocity of the galaxy $v_{\mathrm{esc}} = 544\,\mathrm{km/s}$ [87] is neglected, as these are assumed to largely have left the galaxy. This gives

$$f_{\mathrm{galaxy}}(\mathbf{v}) = \frac{1}{N} \exp\left[-\frac{\mathbf{v}^2}{v_0^2}\right] \Theta\left(v_{\mathrm{esc}} - |\mathbf{v}|\right) , \tag{4.1}$$

which is the DM velocity distribution in the galactic rest frame, with N being a normalisation factor. The Earth moves relative to the galactic rest frame with a velocity $\mathbf{v}_e$. In this thesis we will use $v_e = 250.5\,\mathrm{km/s}$ [87], although several other (similar) values are being used by the DM community. This means that the velocity distribution of the DM particles reaching Earth is

shifted to become

$$f_\chi(\mathbf{v}) = \frac{1}{N_{\text{esc}}\pi^{3/2}v_0^3}\exp\left[-\frac{(\mathbf{v}+\mathbf{v}_e)^2}{v_0^2}\right]\Theta\left(v_{\text{esc}}-|\mathbf{v}+\mathbf{v}_e|\right)\,, \tag{4.2}$$

with

$$N_{\text{esc}} \equiv \text{erf}(v_{\text{esc}}/v_0) - 2(v_{\text{esc}}/v_0)\exp\left[-v_{\text{esc}}^2/v_0^2\right]/\sqrt{\pi}\,, \tag{4.3}$$

being the normalisation factor and erf being the error function. Note that the distribution in eq. (4.2) is skewed in the direction of $-\mathbf{v}_e$, which is usually referred to as the direction of the DM wind.

Another important property of DM is the local DM density ρ_χ, i.e. the density of DM in the vicinity of Earth. In this thesis $\rho_\chi = 0.4\,\text{GeV/cm}^3$ is used, a value compatible with the findings of ref. [88], where $\rho_\chi = 0.385 \pm 0.027\,\text{GeV/cm}^3$ and $\rho_\chi = 0.389 \pm 0.025\,\text{GeV/cm}^3$ was found, depending on the assumed overall DM density profile. Other authors in the DM community are using $\rho_\chi = 0.3\,\text{GeV/cm}^3$ to ensure conservative results.

4.2 Nuclear Recoils

If dark matter scatters elastically with a nucleus, it deposits momentum and energy to the nucleus, causing it to recoil. Most direct detection experiments are designed to detect such nuclear recoils. As the nucleus has a mass of several GeV and the velocity of DM in the vicinity of Earth is of order 10^{-3} in natural units, a DM particle of similar mass to that of the nucleus can deposit energies in the keV range. Specifically, the nucleus has a negligible initial state kinetic energy in the lab frame, and recoils with an energy given as [89]

$$E' = \frac{\mu_{\chi N}^2 v^2}{m_N}\left(1-\cos\theta_R\right)\,, \tag{4.4}$$

where $\mu_{\chi N}$ is the reduced mass of the DM-nucleus system, v is the velocity of the incoming DM particle, m_N is the mass of the nucleus and θ_R is the angle between the path of the recoiled nucleus and that of the incoming DM particle. The rate of these nuclear recoils is then given as

$$\frac{\mathrm{d}\,R}{\mathrm{d}\,E'} = \frac{\rho_\chi}{m_\chi m_N}\int \mathrm{d}^3\,v\,v f_\chi(\mathbf{v})\frac{\mathrm{d}\,\sigma_{\chi N}}{\mathrm{d}\,E'}\,, \tag{4.5}$$

where $\sigma_{\chi N}$ is the DM nucleus scattering cross section.

Spin (in)dependent interactions

One usually takes the cross section to consist of a spin dependent (SD) and a spin independent (SI) term,

$$\frac{\mathrm{d}\,\sigma_{\chi N}}{\mathrm{d}\,E'} = \frac{m_N}{2\mu_{\chi N}^2 v^2}\left[\sigma_{\chi N}^{SI} F_{SI}^2 + \sigma_{\chi N}^{SD} F_{SD}^2\right] , \tag{4.6}$$

where $\sigma_{\chi N}^{SI}$ and $\sigma_{\chi N}^{SD}$ are the spin independent and spin dependent interaction cross sections respectively. They are given as

$$\sigma_{\chi N}^{SI} = \frac{4\mu_{\chi N}^2}{\pi}\left[Z f_p + (A-Z) f_n\right]^2 , \tag{4.7a}$$

$$\sigma_{\chi N}^{SD} = \frac{32 G_F \mu_{\chi N}^2}{\pi}\frac{J+1}{J}\left[a_p\langle S_p\rangle + a_n\langle S_n\rangle\right]^2 , \tag{4.7b}$$

with f_p (a_p) and f_n (a_n) being the spin independent (dependent) coupling of DM to the protons and the neutrons, respectively. $\langle S_p\rangle$ and $\langle S_n\rangle$ are proton and neutron spin factors.

Finally, F_{SI} and F_{SD} are the nuclear form factors [90]. They are introduced to account for the complicating fact that nuclei are not elementary particles; They have an internal structure which, depending on the momentum transfer, can be probed in a scattering with DM. A popular approximation for F_{SI} is the Helm form factor [91], given as

$$F_{SI} \approx F_{\mathrm{Helm}} = \left(\frac{3 j_1\left(q R_1\right)}{q R_1}\right)^2 e^{-q^2 s^2/2} , \tag{4.8}$$

where j_1 is the spherical Bessel function, q is the transferred momentum from the DM particle to the recoiling nucleus, $s \approx 1\,\mathrm{fm}$ is the nuclear skin thickness and $R_1 \approx 1.25 A^{1/3}\,\mathrm{fm}$ is the effective nuclear radius. For a review of nuclear recoils, see [89].

Non-relativistic effective field theory

A more general description of the interaction between DM and the nucleus is that of non-relativistic effective field theory. This framework is developed by

$\mathcal{O}_1 = \mathbb{1}_{\chi e}$	$\mathcal{O}_{11} = i\mathbf{S}_\chi \cdot \frac{\mathbf{q}}{m_e}$
$\mathcal{O}_3 = i\mathbf{S}_e \cdot \left(\frac{\mathbf{q}}{m_e} \times \mathbf{v}_{\rm el}^\perp\right)$	$\mathcal{O}_{12} = \mathbf{S}_\chi \cdot \left(\mathbf{S}_e \times \mathbf{v}_{\rm el}^\perp\right)$
$\mathcal{O}_4 = \mathbf{S}_\chi \cdot \mathbf{S}_e$	$\mathcal{O}_{13} = i\left(\mathbf{S}_\chi \cdot \mathbf{v}_{\rm el}^\perp\right)\left(\mathbf{S}_e \cdot \frac{\mathbf{q}}{m_e}\right)$
$\mathcal{O}_5 = i\mathbf{S}_\chi \cdot \left(\frac{\mathbf{q}}{m_e} \times \mathbf{v}_{\rm el}^\perp\right)$	$\mathcal{O}_{14} = i\left(\mathbf{S}_\chi \cdot \frac{\mathbf{q}}{m_e}\right)\left(\mathbf{S}_e \cdot \mathbf{v}_{\rm el}^\perp\right)$
$\mathcal{O}_6 = \left(\mathbf{S}_\chi \cdot \frac{\mathbf{q}}{m_e}\right)\left(\mathbf{S}_e \cdot \frac{\hat{\mathbf{q}}}{m_e}\right)$	$\mathcal{O}_{15} = i\mathcal{O}_{11}\left[\left(\mathbf{S}_e \times \mathbf{v}_{\rm el}^\perp\right) \cdot \frac{\mathbf{q}}{m_e}\right]$
$\mathcal{O}_7 = \mathbf{S}_e \cdot \mathbf{v}_{\rm el}^\perp$	$\mathcal{O}_{17} = i\frac{\mathbf{q}}{m_e} \cdot \boldsymbol{\mathcal{S}} \cdot \mathbf{v}_{\rm el}^\perp$
$\mathcal{O}_8 = \mathbf{S}_\chi \cdot \mathbf{v}_{\rm el}^\perp$	$\mathcal{O}_{18} = i\frac{\mathbf{q}}{m_e} \cdot \boldsymbol{\mathcal{S}} \cdot \mathbf{S}_e$
$\mathcal{O}_9 = i\mathbf{S}_\chi \cdot \left(\mathbf{S}_e \times \frac{\mathbf{q}}{m_e}\right)$	$\mathcal{O}_{19} = \frac{\mathbf{q}}{m_e} \cdot \boldsymbol{\mathcal{S}} \cdot \frac{\mathbf{q}}{m_e}$
$\mathcal{O}_{10} = i\mathbf{S}_e \cdot \frac{\mathbf{q}}{m_e}$	$\mathcal{O}_{20} = \left(\mathbf{S}_e \times \frac{\mathbf{q}}{m_e}\right) \cdot \boldsymbol{\mathcal{S}} \cdot \frac{\mathbf{q}}{m_e}$

Table 4.1: Interaction operators spanning the non-relativistic effective theory of spin 1/2 DM-electron interactions [63], [65], [92]. $\mathbf{S}_e$ ($\mathbf{S}_\chi$) is the electron (DM) spin, $\mathbf{v}_{\rm el}^\perp = \mathbf{v} - \boldsymbol{\ell}/m_e - \mathbf{q}/(2\mu_{\chi e})$, where $\mu_{\chi e}$ is the DM-electron reduced mass, $\mathbf{v}_{\rm el}^\perp$ is the transverse relative velocity and $\mathbb{1}_{\chi e}$ is the identity in the DM-electron spin space. Finally, $\boldsymbol{\mathcal{S}}$ is the vector DM polarization matrix, and arises in models of spin 1 DM.

considering all possible Lorentz invariant interactions between DM and the nucleus, and then taking the non-relativistic limit by expanding in q/m_n and v, where m_n is the nucleon mass. q/m_n and v are both numbers much smaller than one as the DM particles that are gravitationally bound in the galaxy are non-relativistic. Below this framework will be presented and discussed in the context DM electron scattering, although it first was developed to describe nuclear recoils.[63]

4.3 Electron Recoils from NR-EFT

Electron recoils can be generated from DM in two different ways; through the Migdal Effect [93], [94] by which a DM induced nuclear recoil is converted into an electron recoil; and through DM scattering directly off the electron, the latter of which will be discussed here. The rate at which DM scatters electrons from an initial state 1 into a final state 2 is given as [65]

$$\mathscr{R}_{1\to 2} = \frac{n_\chi}{16 m_\chi^2 m_e^2} \int \frac{\mathrm{d}^3 q}{(2\pi)^3} \int \mathrm{d}^3 v f_\chi(\mathbf{v})(2\pi)\delta(E_f - E_i)\overline{|\mathcal{M}_{1\to 2}|^2}\,, \qquad (4.9)$$

where $n_\chi = \rho_\chi / m_\chi$ is the local number density of DM particles, m_χ is the mass of the DM particle, $\mathbf{q}$ is the momentum transfered from the DM particle to the electron, and E_i and E_f is the initial and final energy of the DM-electron system, respectively. Finally, $\overline{|\mathcal{M}_{1\to2}|^2}$ is the squared electron transition amplitude, given in terms of the initial state electron wave-function ψ_1, the final state electron wave-function ψ_2 and the free scattering amplitude $\mathcal{M}$ as [65]

$$\overline{|\mathcal{M}_{1\to2}|^2} \equiv \overline{\left| \int \frac{\mathrm{d}^3 p_e}{(2\pi)^3} \, \psi_2^*(\mathbf{p}_e + \mathbf{q}) \mathcal{M}(\mathbf{p}_e, \mathbf{p}_\chi, \mathbf{q}) \psi_1(\mathbf{p}_e) \right|^2} , \tag{4.10}$$

where $\mathbf{p}_e$ and $\mathbf{p}_\chi$ is the initial state momentum of the electron and DM particle, respectively. For the dark photon model discussed in section 3.1, $\mathcal{M} = c_1^s$ ($\mathcal{M} = c_1^\ell q_{\mathrm{ref}}^2 / q^2$) for a heavy (light) dark photon, and c_1^s (c_1^ℓ) is the coupling parameter between DM and the electron. In general $\mathcal{M}$ can be expanded in effective operators as

$$\mathcal{M}(\mathbf{q}, \mathbf{v}_{\mathrm{el}}^\perp) = \sum_i \left(c_i^s + c_i^\ell \frac{q_{\mathrm{ref}}^2}{|\mathbf{q}|^2} \right) \langle \mathcal{O}_i \rangle \, , \tag{4.11}$$

where c_i^s and c_i^ℓ are the short and long range[3] coupling parameters, $\mathcal{O}_i$ is the effective operator shown in table 4.1. This expansion in effective operators covers all possible interactions a non-relativistic spin 0 and 1/2 DM particle can have with an electron [63], [65], [92].

Electrons bound in materials have a velocity of order $v = p_e / m_e \sim \alpha Z_{\mathrm{eff}} \approx Z_{\mathrm{eff}}/137$, with Z_{eff} being of order a few for electrons relevant to direct detection experiments. One can therefore Taylor expand the matrix element to first order in $\mathbf{p}_e / m_e$;

$$\mathcal{M} = \mathcal{M}|_{\mathbf{p}_e/m_e=0} + \frac{\mathbf{p}_e}{m_e} \cdot m_e \nabla_{\mathbf{p}_e} \mathcal{M}|_{\mathbf{p}_e/m_e=0} \, . \tag{4.12}$$

[3] All that you touch, and all that you see...

This expansion can now be inserted in eq. (4.10) to obtain

$$\begin{aligned}\overline{|\mathcal{M}_{1\to2}|^2} =& \overline{\left|\mathcal{M}|_{\mathbf{p}_e/m_e=0}\right|^2}\,|f_{1\to2}|^2 \\ &+ 2m_e\overline{\Re\left[\mathcal{M}f_{1\to2}(\nabla_{\mathbf{p}_e}\mathcal{M}^*)|_{\mathbf{p}_e/m_e=0}\cdot(\mathbf{f}_{1\to2})^*\right]} \\ &+ m_e^2\overline{\left|(\nabla_{\mathbf{p}_e}\mathcal{M})|_{\mathbf{p}_e/m_e=0}\cdot\mathbf{f}_{1\to2}\right|^2}\,,\end{aligned} \tag{4.13}$$

where the electron wave-function overlap integrals $f_{1\to2}$ and $\mathbf{f}_{1\to2}$ are given as

$$f_{1\to2} = \int \mathrm{d}^3x\,\psi_2^*(\mathbf{x})e^{i\mathbf{x}\cdot\mathbf{q}}\psi_1(\mathbf{x})\,, \tag{4.14a}$$

$$\mathbf{f}_{1\to2} = \int \mathrm{d}^3x\,\psi_2^*(\mathbf{x})e^{i\mathbf{x}\cdot\mathbf{q}}\frac{i\nabla_{\mathbf{x}}}{m_e}\psi_1(\mathbf{x})\,. \tag{4.14b}$$

In Paper 1, we show that the rate of DM induced electron excitations in semiconductors eq. (4.13) can be written as a sum of 7 products of DM and material response functions[4]. The DM response functions are functions of DM parameters such as the coupling constants c_i^s and c_i^ℓ from eq. (4.11), the transferred momentum $\mathbf{q}$, deposited energy ΔE and the velocity of the incoming DM particle v_χ. On the other hand, the material response functions depend on material properties such as lattice momentum and band energies.

Electron excitation in periodic systems

For processes in which DM causes the electron to be excited from an initial ground state to an excited state, both the initial and final state wave-function is on Bloch form [95], i.e.

$$\psi_{i\mathbf{k}}(\mathbf{x}) = \frac{1}{\sqrt{V}}\sum_{\mathbf{G}} u_i(\mathbf{k}+\mathbf{G})e^{i(\mathbf{k}+\mathbf{G})\cdot\mathbf{x}}\,, \tag{4.15}$$

with i being the band index, $\mathbf{k}$ being the Brillouin zone momentum, $\mathbf{G}$ being the reciprocal lattice vector and V being the volume of the electron system.

[4]The result holds for electron excitations in all periodic systems. We show that two of these products vanish when integration over velocity is performed with the so-called simplified velocity distribution in which the DM velocity distribution is approximated as isotropic in the lab frame.

$u_i(\mathbf{k}+\mathbf{G})$ are the Bloch coefficients, normalized such that $\sum_{\mathbf{G}} |u_i(\mathbf{k}+\mathbf{G})|^2 = 1$ for all i and $\mathbf{k}$. As shown in Paper 1, inserting these wave-functions in eq. (4.14) gives

$$f_{i,\mathbf{k}\to i',\mathbf{k}'} = \sum_{\mathbf{G}\mathbf{G}'} \frac{u^*_{i',\mathbf{k}'} u_{i,\mathbf{k}}}{V} (2\pi)^3 \delta^3(\mathbf{k}+\mathbf{G}+\mathbf{q}-\mathbf{k}'-\mathbf{G}') \,, \tag{4.16a}$$

$$\mathbf{f}_{i,\mathbf{k}\to i',\mathbf{k}'} = -\sum_{\mathbf{G}\mathbf{G}'} \frac{u^*_{i',\mathbf{k}'} u_{i,\mathbf{k}}}{m_e V} (\mathbf{k}+\mathbf{G}) (2\pi)^3 \delta^3(\mathbf{k}+\mathbf{G}+\mathbf{q}-\mathbf{k}'-\mathbf{G}') \,, \tag{4.16b}$$

where the unprimed band indexes, brillouin zone momenta and reciprocal lattice vectors denote the initial state whereas the primed ones denote the final state. Inserting eq. (4.16) into eq. (4.13) gives

$$\begin{aligned}
\overline{|\mathcal{M}_{i,\mathbf{k}\to i',\mathbf{k}'}|^2} = &\sum_{\Delta\mathbf{G}} \frac{(2\pi)^3 \delta^3(\mathbf{k}+\mathbf{q}-\mathbf{k}'-\Delta\mathbf{G})}{V} \Bigg\{ \overline{|\mathcal{M}|^2} \left| f'_{i,\mathbf{k}\to i',\mathbf{k}'} \right|^2 \\
&+ 2m_e \overline{\Re\left[\mathcal{M} f'_{i,\mathbf{k}\to i',\mathbf{k}'} (\nabla_{\mathbf{p}_1} \mathcal{M}^*)_{\mathbf{p}_1=0} \cdot \left(\mathbf{f}'_{i,\mathbf{k}\to i',\mathbf{k}'} \right)^* \right]} \\
&+ m_e^2 \overline{\left| (\nabla_{\mathbf{p}_1} \mathcal{M})_{\mathbf{p}_1=0} \cdot \mathbf{f}'_{i,\mathbf{k}\to i',\mathbf{k}'} \right|^2} \Bigg\} \\
\equiv &\sum_{\Delta\mathbf{G}} \frac{(2\pi)^3 \delta^3(\mathbf{k}+\mathbf{q}-\mathbf{k}'-\Delta\mathbf{G})}{V} \times \overline{\left| \mathcal{M}'_{i,\mathbf{k}\to i',\mathbf{k}'} \right|^2} \,,
\end{aligned} \tag{4.17}$$

with the primed electron wave-function overlap integrals being defined as

$$f'_{i,\mathbf{k}\to i',\mathbf{k}'} \equiv \sum_{\mathbf{G}} u^*_{i'} \left(\mathbf{k}' + \mathbf{G} + \Delta\mathbf{G} \right) u_i \left(\mathbf{k} + \mathbf{G} \right) \,, \tag{4.18a}$$

$$\mathbf{f}'_{i,\mathbf{k}\to i',\mathbf{k}'} \equiv -\frac{1}{m_e} \sum_{\mathbf{G}} u^*_{i'} \left(\mathbf{k}' + \mathbf{G} + \Delta\mathbf{G} \right) \left(\mathbf{k} + \mathbf{G} \right) u_i \left(\mathbf{k} + \mathbf{G} \right) \,. \tag{4.18b}$$

Eq. (4.9) gives the rate of scattering from an initial state $1 \to \{i, \mathbf{k}\}$ to a final state $2 \to \{i', \mathbf{k}'\}$. The total rate of excitations is obtained by summing over i and i', and integrating over $\mathbf{k}$ and $\mathbf{k}'$:

$$\mathscr{R} = 2 \sum_{ii'} \int_{\mathrm{BZ}} \frac{V \mathrm{d}^3 k}{(2\pi)^3} \int_{\mathrm{BZ}} \frac{V \mathrm{d}^3 k'}{(2\pi)^3} \mathscr{R}_{i\mathbf{k}\to i'\mathbf{k}'} \,, \tag{4.19}$$

$B_1 = \left\lvert f'_{i,\mathbf{k}\to i',\mathbf{k}'}\right\rvert^2$	$B_5 = i\frac{\mathbf{q}}{m_e}\cdot\left[\mathbf{f}'_{i,\mathbf{k}\to i',\mathbf{k}'}\times\left(\mathbf{f}'_{i,\mathbf{k}\to i',\mathbf{k}'}\right)^*\right]$
$B_2 = \frac{\mathbf{q}}{m_e}\cdot(f'_{i,\mathbf{k}\to i',\mathbf{k}'})(\mathbf{f}'_{i,\mathbf{k}\to i',\mathbf{k}'})^*$	$\mathbf{B}_6 = f'_{i,\mathbf{k}\to i',\mathbf{k}'}\left(\mathbf{f}'_{i,\mathbf{k}\to i',\mathbf{k}'}\right)^*$
$B_3 = \left\lvert\mathbf{f}'_{i,\mathbf{k}\to i',\mathbf{k}'}\right\rvert^2$	$\mathbf{B}_7 = \frac{\mathbf{q}}{m_e}\times f'_{i,\mathbf{k}\to i',\mathbf{k}'}\left(\mathbf{f}'_{i,\mathbf{k}\to i',\mathbf{k}'}\right)^*$
$B_4 = \left\lvert\frac{\mathbf{q}}{m_e}\cdot\mathbf{f}'_{i,\mathbf{k}\to i',\mathbf{k}'}\right\rvert^2$	

Table 4.2: Products of electron wave-function overlap integrals generating the material response functions.

where the factor of 2 in front accounts for there being 2 electrons in every initial state band i. Inserting eqs. (4.9) and (4.17) into the above equation gives

$$\begin{aligned}\mathscr{R} = &\frac{\pi n_\chi V}{4m_\chi^2 m_e^2}\int \mathrm{d}^3q \int \mathrm{d}^3v\, f_\chi(\mathbf{v})\delta\left(E_{i'\mathbf{k}'} - E_{i\mathbf{k}} + \frac{q^2}{2m_\chi} - \mathbf{q}\cdot\mathbf{v}\right)\\ &\times\sum_{\Delta\mathbf{G}ii'}\int_{\mathrm{BZ}}\frac{\mathrm{d}^3k}{(2\pi)^3}\int_{\mathrm{BZ}}\frac{\mathrm{d}^3k'}{(2\pi)^3}\overline{\left\lvert\mathcal{M}'_{i,\mathbf{k}\to i',\mathbf{k}'}\right\rvert^2}\delta^3(\mathbf{k}+\mathbf{q}-\mathbf{k}'-\Delta\mathbf{G})\,. \qquad (4.20)\end{aligned}$$

Rearranging the above equation and introducing an integral over ΔE together with $\delta(\Delta E - E_{i\mathbf{k}} + E_{i'\mathbf{k}'})$ the above equation can be written as

$$\begin{aligned}\mathscr{R} = &\frac{n_\chi N_{\mathrm{cell}}}{64\pi m_\chi^2 m_e^2}\int \mathrm{d}^3q \int \mathrm{d}\,\ln(\Delta E)\int \mathrm{d}^3v\, f_\chi(\mathbf{v})\delta\left(\Delta E + \frac{q^2}{2m_\chi} - \mathbf{q}\cdot\mathbf{v}\right)\\ &\times\sum_{l=1}^{r}\Re\left(R_l^*(q,v)W_l(\mathbf{q},\Delta E)\right) \qquad (4.21)\end{aligned}$$

where R_l is the dark matter response function, and the material physics is contained within W_l defined as

$$\begin{aligned}W_l(\mathbf{q},\Delta E) = &(4\pi)^2 V_{\mathrm{cell}}\Delta E\sum_{\Delta\mathbf{G}ii'}\int_{\mathrm{BZ}}\frac{\mathrm{d}^3k}{(2\pi)^3}\int_{\mathrm{BZ}}\frac{\mathrm{d}^3k'}{(2\pi)^3}\,B_l\\ &\times\delta^3(\mathbf{q}-\mathbf{k}'-\Delta\mathbf{G}+\mathbf{k})\delta(\Delta E - E_{i\mathbf{k}} + E_{i'\mathbf{k}'})\,. \qquad (4.22)\end{aligned}$$

B_l are functions built from the electron wave function overlap integrals in eq. (4.18), given in tab. 4.2.

The material response functions in eqs. (4.22) depend on sums over bands and reciprocal lattice vectors, and integrals over Brillouin zone momentum of Bloch coefficients u. In Paper 1, W is computed using Density Functional Theory (DFT), which is reviewed in the next chapter.

CHAPTER 5

Density Functional Theory

For several applications ranging from biology, medicine and chemistry to material science, computer chips and dark matter direct detection experiments, understanding the electronic structure in molecules and solids is crucial. The electronic structure is described by the many-body Schrödinger equation, and solving it for various systems is therefore a central problem in (low energy) physics. The relevant system to describe a solid is that of $n_e \sim 10^{24}$ electrons all interacting with each other and with an almost as large number of nuclei. Accounting for all these particles and all the interactions between them is computationally impossible. Density Functional Theory (DFT) overcomes this by introducing an electron density experiencing an effective potential. In this chapter a brief overview of DFT will be given.

5.1 Kohn, Sham and exchange-correlation energies

A set of central equations in DFT are the Kohn-Sham equations from ref. [96],

$$E = -\frac{1}{2}\sum_i \int \mathrm{d}^3\, x\, \psi_i^*(\mathbf{x})\nabla^2\psi_i(\mathbf{x}) + \frac{1}{2}\int \mathrm{d}^3\, x\, \mathrm{d}^3\, x'\, \frac{n_e(\mathbf{x})n_e(\mathbf{x}')}{|\mathbf{x}-\mathbf{x}'|} + \int \mathrm{d}^3\, x \left[V_{\mathrm{ext}}(\mathbf{x}) + \epsilon_{xc}\left(n_e^{\uparrow}(\mathbf{x}), n_e^{\downarrow}(\mathbf{x})\right)\right] n_e(\mathbf{x})\,, \tag{5.1a}$$

$$\epsilon_i\psi_i(\mathbf{x}) = \left\{-\frac{1}{2}\nabla^2 + V_{\mathrm{ext}}(\mathbf{x}) + \int \mathrm{d}^3\, x'\, \frac{n_e\left(\mathbf{x}'\right)}{|\mathbf{x}-\mathbf{x}'|} + \frac{\mathrm{d}}{\mathrm{d}n_e}\left(n_e\epsilon_{xc}(n_e)\right)\right\}\psi_i(\mathbf{x})\,, \tag{5.1b}$$

$$n_e(\mathbf{x}) = \sum_i |\psi_i(\mathbf{x})|^2\,, \tag{5.1c}$$

where E is the energy of the electron system, which can be minimized to obtain the ground state. $n_e(\mathbf{x}) = n_e^{\uparrow}(\mathbf{x}) + n_e^{\downarrow}(\mathbf{x})$ is the electron number density of the system with $n_e^{\uparrow}(\mathbf{x})$ and $n_e^{\downarrow}(\mathbf{x})$ being the density of spin up and spin down electrons respectively. ψ_i are orthogonal Kohn-Sham orbitals with energy ϵ_i, and $V_{\mathrm{ext}}(\mathbf{x})$ the external potential experienced by the electrons. The Kohn-Sham orbitals have the advantage that they can be calculated from eq. (5.1b), which is similar to the 1 particle Schrödinger equation. Finally, ϵ_{xc} is known as the exchange and correlation energy per electron, taking quantum effects into account and making the 3 last terms in eq. (5.1b) an effective potential. As a first approximation in ref. [96], Kohn and Sham took $\epsilon_{xc}\left(n_e^{\uparrow}(\mathbf{x}), n_e^{\downarrow}(\mathbf{x})\right)$ to be that of a free electron gas of density n_e. This approximation for ϵ_{xc} is known as the Local Spin Density (LSD) approximation.

Another more accurate approximation for the exchange and correlation energy is that of Generalized Gradient Approximation (GGA) [97], in which the exchange and correlation energy is allowed to also depend on the gradient of the electron density, that is

$$\epsilon_{xc} = \epsilon_{xc}^{GGA}\left(n_e^{\uparrow}(\mathbf{x}), n_e^{\downarrow}(\mathbf{x}), \nabla n_e^{\uparrow}(\mathbf{x}), \nabla n_e^{\downarrow}(\mathbf{x})\right)\,. \tag{5.2}$$

GGA does in general perform better than LSD, although the exchange and correlation energy under the GGA approximation is more complicated and difficult to obtain. In Paper 1 we use pseudopotentials obtained with GGA.

5.2 Plane Wave Self-consistent DFT calculation

When obtaining the material response functions in eq. (4.22), the ground state electron wave-functions have to be found. This can be done using a self-consistent DFT calculation. One then iteratively solve the Kohn-Sham equations (5.1) to find a converged $n_e(\mathbf{x})$. The Kohn-Sham orbitals are expanded in terms of plane waves using the Bloch Theorem [95],

$$\psi_{i,\mathbf{k}}(\mathbf{x}) = \frac{1}{\sqrt{V}} \sum_{\mathbf{G}} u_i(\mathbf{k}+\mathbf{G})\, e^{i(\mathbf{k}+\mathbf{G})\cdot\mathbf{x}}\,, \tag{5.3}$$

where the number of plane waves included is set by the cut-off energy E_{cut}, by the relation

$$\frac{(\mathbf{k}+\mathbf{G})^2}{2m_e} \leq E_{\text{cut}}\,. \tag{5.4}$$

In particular, one iteratively go through the self consistency loop [98]:

$$\epsilon_i^{(n)}\psi_i^{(n)}(\mathbf{x}) = \left\{-\frac{1}{2}\nabla^2 + V_{\text{in}}^{(n)}(\mathbf{x})\right\}\psi_i^{(n)}(\mathbf{x})\,, \tag{5.5a}$$

$$n_e^{(n)}(\mathbf{x}) = \sum_i \left|\psi_i^{(n)}(\mathbf{x})\right|^2\,, \tag{5.5b}$$

$$V_{\text{out}}^{(n)}(\mathbf{x}) = V_{\text{ext}}(\mathbf{x}) + \int \mathrm{d}^3\, x'\, \frac{n_e^{(n)}(\mathbf{x}')}{|\mathbf{x}-\mathbf{x}'|} + \frac{\mathrm{d}}{\mathrm{d}n_e^{(n)}}\left(n_e^{(n)}\epsilon_{xc}(n_e^{(n)})\right)\,, \tag{5.5c}$$

where one could take $V_{\text{in}}^{(n+1)} = V_{\text{out}}^{(n)}$, although it has proven more efficient to take $V_{\text{in}}^{(n+1)} = (1-\beta)V_{\text{in}}^{(n)} + \beta V_{\text{out}}^{(n)}$ with β being a parameter valued between 0 and 1. V_{ext} is provided by an external Pseudo Potential, which allows for the electron orbitals closest to the nucleus[1] to be included in the external potential. One then does not need to obtain the Kohn-Sham orbitals for these core electrons. The iteration loop in eq. (5.5) is being carried out by `Quantum ESPRESSO` [99]–[101], which recasts eq. (5.5a) into a linear algebra eigenvalue problem and solves it, obtaining the Bloch coefficients, $u_i(\mathbf{k}+\mathbf{G})$. These can in turn be used to compute the material response functions in eq. (4.22), which is done in the `QEdark-EFT` code [102], described below.

[1] Often referred to as core electrons or core states

5.3 QEdark-EFT

QEdark-EFT builds on QEdark [58], and computes W_l from eq. (4.22) for all l. This is done by discretication, which converts the delta functions in the definition of W_l into Heaviside functions, and the integrals over Brillouin zone momentum into sums over discrete points. The Heaviside functions serve as bins in energy and momentum, and QEdark-EFT loops over the discreticed Brillouin zone momentum, bands and reciprocal lattice vectors. For each combination of these, $u_i(\mathbf{k}+\mathbf{G})$ which have been precomputed in a self-consistent DFT calculation performed with Quantum ESPRESSO is loaded and used to compute B_l. The contribution to W_l is then added to the bin identified from the band energy, Brillouin zone momentum and reciprocal lattice vector. The code then outputs W_l for a grid of momentum and energy. This W-grid is then loaded by a separate code which performs the integrals in eq. (4.21) to obtain the rates of electron-hole pair creation. The former of these codes was extended whereas the latter was written from scratch by the author of this thesis during the work on Paper 1.

CHAPTER 6

Summary and Outlook

The nature of dark matter is one of the greatest unanswered questions in modern particle physics, and answering it requires both experimental and theoretical efforts. With the emergence of DD experiments sensitive to DM-electron scatterings, a theoretical understanding of these scatterings is crucial, not just for the benchmark case of the interaction being mediated by a dark photon mixing with the visible one, but for general forms of interactions. The description of DM-electron scatterings is complicated by the electron being bound. This gives rise to a rich phenomenology at the interface between theoretical particle physics and theoretical condensed matter physics. In Paper 1 we model DM induced electronic excitations in crystals for general fermionic DM electron interactions. We find that depending on the nature of the DM-electron interaction as many as 7 different crystal responses can be induced. 6 of these ways in which crystals can respond to an outer probe were theorised for the first time in Paper 1. We also present expected rates of DM induced electron-hole pair production for various models of DM, and use existing experimental data to constrain the parameters of the models.

In Paper 2, we expand the work to also include bosonic DM with spin 1. While spin 1 DM does not produce crystal responses different to the ones pro-

duced by spin 0 and 1/2 DM, the work demonstrates how these novel crystal responses generically appear in models of DM. This is done by considering a wide range of simplified models, and showing that the novel responses from Paper 1 arise in many of them. It thus demonstrates the importance of taking all crystal responses into account when interpreting results of silicon and germanium based experiments.

In the future, the work conducted on silicon and germanium will be extended to also cover other materials, such as graphene and liquid xenon. Graphene is interesting to cover due to its anisotropy, making it sensitive to the direction from which dark matter came. This can help confirm that an observed DM electron scattering really is due to DM and not an unknown or misunderstood background source. Liquid xenon, on the other hand, is interesting to look at because it is being used in very large and sensitive DD experiments. Previously, the response of isolated xenon atoms to general interactions with DM have been calculated in [65], and the xenon atoms have been taken as a proxy for liquid xenon. Using isolated atoms as a proxy for a liquid does however miss the impact of atom-atom interactions in the liquid. This is expected to alter the initial state electron wave function somewhat, which again will have an impact on the expected rate of DM electron scatterings. An interesting difference between these projects and the work carried out in Paper 1 is that whereas the work in Paper 1 models creation of electron hole pairs, the upcoming works will treat electrons being ejected from the material.

References

[1] N. Aghanim *et al.*, "Planck 2018 results. VI. Cosmological parameters," *Astron. Astrophys.*, vol. 641, A6, 2020, [Erratum: Astron.Astrophys. 652, C4 (2021)].

[2] D. N. Spergel *et al.*, "First year Wilkinson Microwave Anisotropy Probe (WMAP) observations: Determination of cosmological parameters," *Astrophys. J. Suppl.*, vol. 148, pp. 175–194, 2003.

[3] N. Aghanim *et al.*, "Planck 2018 results. I. Overview and the cosmological legacy of Planck," *Astron. Astrophys.*, vol. 641, A1, 2020.

[4] G. Bertone and D. Hooper, "History of dark matter," *Rev. Mod. Phys.*, vol. 90, no. 4, p. 045 002, 2018.

[5] B. J. Carr, "The Primordial black hole mass spectrum," *Astrophys. J.*, vol. 201, pp. 1–19, 1975.

[6] S. W. Hawking, "Black hole explosions," *Nature*, vol. 248, pp. 30–31, 1974.

[7] ——, "Particle Creation by Black Holes," *Commun. Math. Phys.*, vol. 43, G. W. Gibbons and S. W. Hawking, Eds., pp. 199–220, 1975, [Erratum: Commun.Math.Phys. 46, 206 (1976)].

[8] B. Carr, F. Kuhnel, and M. Sandstad, "Primordial Black Holes as Dark Matter," *Phys. Rev. D*, vol. 94, no. 8, p. 083 504, 2016.

[9] B. P. Abbott *et al.*, "Observation of Gravitational Waves from a Binary Black Hole Merger," *Phys. Rev. Lett.*, vol. 116, no. 6, p. 061 102, 2016.

[10] J. D. Bekenstein, "Relativistic gravitation theory for the modified Newtonian dynamics paradigm," *Phys. Rev. D*, vol. 70, p. 083 509, 8 Oct. 2004.

[11] R. D. Peccei and H. R. Quinn, "Constraints Imposed by CP Conservation in the Presence of Instantons," *Phys. Rev. D*, vol. 16, pp. 1791–1797, 1977.

[12] Peccei, R. D. and Quinn, Helen R., "CP Conservation in the Presence of Instantons," *Phys. Rev. Lett.*, vol. 38, pp. 1440–1443, 1977.

[13] F. Wilczek, "Problem of Strong P and T Invariance in the Presence of Instantons," *Phys. Rev. Lett.*, vol. 40, pp. 279–282, 1978.

[14] S. Weinberg, "A New Light Boson?" *Phys. Rev. Lett.*, vol. 40, pp. 223–226, 1978.

[15] S. Dodelson and L. M. Widrow, "Sterile-neutrinos as dark matter," *Phys. Rev. Lett.*, vol. 72, pp. 17–20, 1994.

[16] Y. Fukuda *et al.*, "Evidence for oscillation of atmospheric neutrinos," *Phys. Rev. Lett.*, vol. 81, pp. 1562–1567, 1998.

[17] M. Apollonio *et al.*, "Limits on neutrino oscillations from the CHOOZ experiment," *Phys. Lett. B*, vol. 466, pp. 415–430, 1999.

[18] J. Schechter and J. W. F. Valle, "Neutrino Masses in SU(2) x U(1) Theories," *Phys. Rev. D*, vol. 22, p. 2227, 1980.

[19] B. Moore, "Evidence against dissipationless dark matter from observations of galaxy haloes," *Nature*, vol. 370, p. 629, 1994.

[20] L. Sagunski, S. Gad-Nasr, B. Colquhoun, A. Robertson, and S. Tulin, "Velocity-dependent Self-interacting Dark Matter from Groups and Clusters of Galaxies," *JCAP*, vol. 01, p. 024, 2021.

[21] X. Li, K. Duan, W. Jiang, Z. Shen, and M. Munoz Salinas, "Recent Gamma-ray Results from DAMPE," *PoS*, vol. ICRC2019, p. 576, 2021.

[22] W. B. Atwood *et al.*, "The Large Area Telescope on the Fermi Gamma-ray Space Telescope Mission," *Astrophys. J.*, vol. 697, pp. 1071–1102, 2009.

[23] F. Aharonian *et al.*, "The h.e.s.s. survey of the inner galaxy in very high-energy gamma-rays," *Astrophys. J.*, vol. 636, pp. 777–797, 2006.

[24] G. Ambrosi *et al.*, "Direct detection of a break in the teraelectronvolt cosmic-ray spectrum of electrons and positrons," *Nature*, vol. 552, pp. 63–66, 2017.

[25] A. A. Abdo *et al.*, "Measurement of the Cosmic Ray e+ plus e- spectrum from 20 GeV to 1 TeV with the Fermi Large Area Telescope," *Phys. Rev. Lett.*, vol. 102, p. 181 101, 2009.

[26] F. Aharonian *et al.*, "The energy spectrum of cosmic-ray electrons at TeV energies," *Phys. Rev. Lett.*, vol. 101, p. 261 104, 2008.

[27] J. Aleksić *et al.*, "The major upgrade of the MAGIC telescopes, Part II: A performance study using observations of the Crab Nebula," *Astropart. Phys.*, vol. 72, pp. 76–94, 2016.

[28] J. Holder *et al.*, "The first VERITAS telescope," *Astropart. Phys.*, vol. 25, pp. 391–401, 2006.

[29] R. Battiston, "The antimatter spectrometer (AMS-02): A particle physics detector in space," *Nucl. Instrum. Meth. A*, vol. 588, A. Capone, M. De Vincenzi, F. Lucarelli, and A. Morselli, Eds., pp. 227–234, 2008.

[30] M. G. Aartsen *et al.*, "Observation of High-Energy Astrophysical Neutrinos in Three Years of IceCube Data," *Phys. Rev. Lett.*, vol. 113, p. 101 101, 2014.

[31] M. Ageron *et al.*, "ANTARES: the first undersea neutrino telescope," *Nucl. Instrum. Meth. A*, vol. 656, pp. 11–38, 2011.

[32] S. Adrián-Martínez *et al.*, "Deep sea tests of a prototype of the KM3NeT digital optical module," *Eur. Phys. J. C*, vol. 74, no. 9, p. 3056, 2014.

[33] G. Aad *et al.*, "Observation of a new particle in the search for the Standard Model Higgs boson with the ATLAS detector at the LHC," *Phys. Lett. B*, vol. 716, pp. 1–29, 2012.

[34] S. Chatrchyan *et al.*, "Observation of a New Boson at a Mass of 125 GeV with the CMS Experiment at the LHC," *Phys. Lett. B*, vol. 716, pp. 30–61, 2012.

[35] G. Aad *et al.*, "Combined Measurement of the Higgs Boson Mass in pp Collisions at $\sqrt{s} = 7$ and 8 TeV with the ATLAS and CMS Experiments," *Phys. Rev. Lett.*, vol. 114, p. 191 803, 2015.

[36] F. Abe *et al.*, "Observation of top quark production in $\bar{p}p$ collisions," *Phys. Rev. Lett.*, vol. 74, pp. 2626–2631, 1995.

[37] S. Abachi *et al.*, "Observation of the top quark," *Phys. Rev. Lett.*, vol. 74, pp. 2632–2637, 1995.

[38] "Combination of CDF and D0 Results on the Mass of the Top Quark," Mar. 2009.

[39] A. Abashian *et al.*, "The Belle Detector," *Nucl. Instrum. Meth. A*, vol. 479, pp. 117–232, 2002.

[40] L. Roszkowski, E. M. Sessolo, and S. Trojanowski, "WIMP dark matter candidates and searches—current status and future prospects," *Rept. Prog. Phys.*, vol. 81, no. 6, p. 066 201, 2018.

[41] E. Aprile, "The XENON1T Dark Matter Search Experiment," *Springer Proc. Phys.*, vol. 148, D. Cline, Ed., pp. 93–96, 2013.

[42] E. Aprile *et al.*, "Projected WIMP sensitivity of the XENONnT dark matter experiment," *JCAP*, vol. 11, p. 031, 2020.

[43] D. S. Akerib *et al.*, "First results from the LUX dark matter experiment at the Sanford Underground Research Facility," *Phys. Rev. Lett.*, vol. 112, p. 091 303, 2014.

[44] J. Aalbers *et al.*, "First Dark Matter Search Results from the LUX-ZEPLIN (LZ) Experiment," Jul. 2022.

[45] P. Agnes *et al.*, "Low-Mass Dark Matter Search with the DarkSide-50 Experiment," *Phys. Rev. Lett.*, vol. 121, no. 8, p. 081 307, 2018.

[46] P. .-A. Amaudruz *et al.*, "Design and Construction of the DEAP-3600 Dark Matter Detector," *Astropart. Phys.*, vol. 108, pp. 1–23, 2019.

[47] A. H. Abdelhameed *et al.*, "First results from the CRESST-III low-mass dark matter program," *Phys. Rev. D*, vol. 100, no. 10, p. 102 002, 2019.

[48] L. Barak *et al.*, "SENSEI: Direct-Detection Results on sub-GeV Dark Matter from a New Skipper-CCD," *Phys. Rev. Lett.*, vol. 125, no. 17, p. 171 802, 2020.

[49] A. Aguilar-Arevalo *et al.*, "Constraints on Light Dark Matter Particles Interacting with Electrons from DAMIC at SNOLAB," *Phys. Rev. Lett.*, vol. 123, no. 18, p. 181 802, 2019.

[50] Q. Arnaud *et al.*, "First germanium-based constraints on sub-MeV Dark Matter with the EDELWEISS experiment," *Phys. Rev. Lett.*, vol. 125, no. 14, p. 141 301, 2020.

[51] R. Agnese *et al.*, "Projected Sensitivity of the SuperCDMS SNOLAB experiment," *Phys. Rev. D*, vol. 95, no. 8, p. 082 002, 2017.

[52] G. Angloher *et al.*, "Results from the first cryogenic NaI detector for the COSINUS project," *JINST*, vol. 12, no. 11, P11007, 2017.

[53] J. Amare *et al.*, "Annual Modulation Results from Three Years Exposure of ANAIS-112," *Phys. Rev. D*, vol. 103, no. 10, p. 102 005, 2021.

[54] R. Bernabei *et al.*, "New results from DAMA/LIBRA," *Eur. Phys. J. C*, vol. 67, pp. 39–49, 2010.

[55] E. Aprile *et al.*, "Excess electronic recoil events in XENON1T," *Phys. Rev. D*, vol. 102, no. 7, p. 072 004, 2020.

[56] ——, "Search for New Physics in Electronic Recoil Data from XENONnT," Jul. 2022.

[57] E. Baracchini *et al.*, "PTOLEMY: A Proposal for Thermal Relic Detection of Massive Neutrinos and Directional Detection of MeV Dark Matter," Aug. 2018.

[58] R. Essig, M. Fernandez-Serra, J. Mardon, A. Soto, T. Volansky, and T.-T. Yu, "Direct Detection of sub-GeV Dark Matter with Semiconductor Targets," *JHEP*, vol. 05, p. 046, 2016.

[59] S. Derenzo, R. Essig, A. Massari, A. Soto, and T.-T. Yu, "Direct Detection of sub-GeV Dark Matter with Scintillating Targets," *Phys. Rev. D*, vol. 96, no. 1, p. 016 026, 2017.

[60] T. Trickle, Z. Zhang, and K. M. Zurek, "Effective field theory of dark matter direct detection with collective excitations," *Phys. Rev. D*, vol. 105, no. 1, p. 015 001, 2022.

[61] S. M. Griffin, K. Inzani, T. Trickle, Z. Zhang, and K. M. Zurek, "Extended calculation of dark matter-electron scattering in crystal targets," *Phys. Rev. D*, vol. 104, no. 9, p. 095 015, 2021.

[62] T. D. Trickle, "Direct Detection of Light Dark Matter with Electrons, Phonons, and Magnons," Ph.D. dissertation, Caltech, 2022.

[63] A. L. Fitzpatrick, W. Haxton, E. Katz, N. Lubbers, and Y. Xu, "The Effective Field Theory of Dark Matter Direct Detection," *JCAP*, vol. 02, p. 004, 2013.

[64] P. Gondolo, S. Kang, S. Scopel, and G. Tomar, "Effective theory of nuclear scattering for a WIMP of arbitrary spin," *Phys. Rev. D*, vol. 104, no. 6, p. 063 017, 2021.

[65] R. Catena, T. Emken, N. A. Spaldin, and W. Tarantino, "Atomic responses to general dark matter-electron interactions," *Phys. Rev. Res.*, vol. 2, no. 3, p. 033 195, 2020.

[66] R. K. Sachs and A. M. Wolfe, "Perturbations of a cosmological model and angular variations of the microwave background," *Astrophys. J.*, vol. 147, pp. 73–90, 1967.

[67] V. Springel, C. S. Frenk, and S. D. M. White, "The large-scale structure of the Universe," *Nature*, vol. 440, p. 1137, 2006.

[68] S. Alam *et al.*, "The Eleventh and Twelfth Data Releases of the Sloan Digital Sky Survey: Final Data from SDSS-III," *Astrophys. J. Suppl.*, vol. 219, no. 1, p. 12, 2015.

[69] S. Alam *et al.*, "The clustering of galaxies in the completed SDSS-III Baryon Oscillation Spectroscopic Survey: cosmological analysis of the DR12 galaxy sample," *Mon. Not. Roy. Astron. Soc.*, vol. 470, no. 3, pp. 2617–2652, 2017.

[70] NASA/STScI; ESO WFI; Magellan/U.Arizona/D.Clowe *et al.*, "Lensing Map of 1E 0657-56,"

[71] NASA/CXC/CfA/M.Markevitch *et al.*, "X-ray Map of 1E 0657-56,"

[72] NASA/STScI; Magellan/U.Arizona/D.Clowe *et al.*, "Optical Map of 1E 0657-56,"

[73] A. Einstein, "The Foundation of the General Theory of Relativity," *Annalen Phys.*, vol. 49, no. 7, J.-P. Hsu and D. Fine, Eds., pp. 769–822, 1916.

[74] H. Katz, F. Lelli, S. S. McGaugh, A. Di Cintio, C. B. Brook, and J. M. Schombert, "Testing feedback-modified dark matter haloes with galaxy rotation curves: estimation of halo parameters and consistency with ΛCDM scaling relations," *Monthly Notices of the Royal Astronomical Society*, vol. 466, no. 2, pp. 1648–1668, Dec. 2016, ISSN: 1365-2966.

[75] E. Hubble and M. L. Humason, "The Velocity-Distance Relation among Extra-Galactic Nebulae," *Astrophys. J.*, vol. 74, pp. 43–80, 1931.

[76] F. Zwicky, "Die Rotverschiebung von extragalaktischen Nebeln," *Helv. Phys. Acta*, vol. 6, pp. 110–127, 1933.

[77] I. Newton, *Philosophiæ Naturalis Principia Mathematica*. England, 1687.

[78] R. Catena, D. Cole, T. Emken, M. Matas, N. Spaldin, W. Tarantino, and E. Urdshals, "Dark matter - electron interactions in materials beyond the dark photon model," Oct. 2022.

[79] C. Abel *et al.*, "Measurement of the Permanent Electric Dipole Moment of the Neutron," *Phys. Rev. Lett.*, vol. 124, no. 8, p. 081 803, 2020.

[80] R. D. Peccei, "The Strong CP problem and axions," *Lect. Notes Phys.*, vol. 741, M. Kuster, G. Raffelt, and B. Beltran, Eds., pp. 3–17, 2008.

[81] C. Vafa and E. Witten, "Restrictions on Symmetry Breaking in Vector-Like Gauge Theories," *Nucl. Phys. B*, vol. 234, pp. 173–188, 1984.

[82] M. Gorghetto and G. Villadoro, "Topological Susceptibility and QCD Axion Mass: QED and NNLO corrections," *JHEP*, vol. 03, p. 033, 2019.

[83] C. B. Adams *et al.*, "Axion Dark Matter," in *2022 Snowmass Summer Study*, Mar. 2022.

[84] D. E. Kaplan, M. A. Luty, and K. M. Zurek, "Asymmetric Dark Matter," *Phys. Rev. D*, vol. 79, p. 115 016, 2009.

[85] L. J. Hall, K. Jedamzik, J. March-Russell, and S. M. West, "Freeze-In Production of FIMP Dark Matter," *JHEP*, vol. 03, p. 080, 2010.

[86] K. Griest and D. Seckel, "Three exceptions in the calculation of relic abundances," *Phys. Rev. D*, vol. 43, pp. 3191–3203, 1991.

[87] D. Baxter *et al.*, "Recommended conventions for reporting results from direct dark matter searches," *Eur. Phys. J. C*, vol. 81, no. 10, p. 907, 2021.

[88] R. Catena and P. Ullio, "A novel determination of the local dark matter density," *JCAP*, vol. 08, p. 004, 2010.

[89] J. Cooley, "Dark Matter direct detection of classical WIMPs," *SciPost Phys. Lect. Notes*, vol. 55, p. 1, 2022.

[90] J. D. Lewin and P. F. Smith, "Review of mathematics, numerical factors, and corrections for dark matter experiments based on elastic nuclear recoil," *Astropart. Phys.*, vol. 6, pp. 87–112, 1996.

[91] R. H. Helm, "Inelastic and Elastic Scattering of 187-Mev Electrons from Selected Even-Even Nuclei," *Phys. Rev.*, vol. 104, pp. 1466–1475, 5 Dec. 1956.

[92] J. Fan, M. Reece, and L.-T. Wang, "Non-relativistic effective theory of dark matter direct detection," *JCAP*, vol. 1011, p. 042, 2010.

[93] A. Migdal, "Ionization of atoms accompanying α- and β-decay.," *J. Phys. USSR*, vol. 4, p. 449, 1941.

[94] M. Ibe, W. Nakano, Y. Shoji, and K. Suzuki, "Migdal Effect in Dark Matter Direct Detection Experiments," *JHEP*, vol. 03, p. 194, 2018.

[95] F. Bloch, "Über die Quantenmechanik der Elektronen in Kristallgittern," *Zeitschrift für Physik*, vol. 52, pp. 555–600,

[96] W. Kohn and L. J. Sham, "Self-Consistent Equations Including Exchange and Correlation Effects," *Phys. Rev.*, vol. 140, A1133–A1138, 4A Nov. 1965.

[97] J. P. Perdew, K. Burke, and M. Ernzerhof, "Generalized Gradient Approximation Made Simple," *Phys. Rev. Lett.*, vol. 77, pp. 3865–3868, 18 Oct. 1996.

[98] A. Dal Corso, "A Pseudopotential Plane Waves Program (PWSCF) and some Case Studies," in *Quantum-Mechanical Ab-initio Calculation of the Properties of Crystalline Materials*, C. Pisani, Ed. Berlin, Heidelberg: Springer Berlin Heidelberg, 1996, pp. 155–178, ISBN: 978-3-642-61478-1.

[99] P. Giannozzi, S. Baroni, N. Bonini, *et al.*, "QUANTUM ESPRESSO: a modular and open-source software project for quantum simulations of materials," *Journal of Physics: Condensed Matter*, vol. 21, no. 39, p. 395 502, Sep. 2009.

[100] P. Giannozzi, O. Andreussi, T. Brumme, *et al.*, "Advanced capabilities for materials modelling with Quantum ESPRESSO," *Journal of Physics: Condensed Matter*, vol. 29, no. 46, p. 465 901, Oct. 2017.

[101] P. Giannozzi, O. Baseggio, P. Bonfà, *et al.*, "Quantum ESPRESSO toward the exascale," *The Journal of Chemical Physics*, vol. 152, no. 15, p. 154 105, 2020.

[102] E. Urdshals and M. Matas, *QEdark-EFT*, version 0.1.0, May 2021.